EUROPEAN RESPIRATORY *journal*

FLAGSHIP SCIENTIFIC JOURNAL OF ERS

Early View

Original article

Fibrocyte accumulation in the airway walls of COPD patients

Isabelle Dupin, Matthieu Thumerel, Elise Maurat, Florence Coste, Edmée Eyraud, Hugues Begueret, Thomas Trian, Michel Montaudon, Roger Marthan, Pierre-Olivier Girodet, Patrick Berger

Please cite this article as: Dupin I, Thumerel M, Maurat E, *et al*. Fibrocyte accumulation in the airway walls of COPD patients. *Eur Respir J* 2019; in press (https://doi.org/10.1183/13993003.02173-2018).

Fibrocyte accumulation in the airway walls of COPD patients

Isabelle Dupin[1,2,*], Matthieu Thumerel[1,2,3,*], Elise Maurat[1,2], Florence Coste[1,2], Edmée Eyraud[1,2], Hugues Begueret[3], Thomas Trian[1,2], Michel Montaudon[1,2,3], Roger Marthan[1,2,3], Pierre-Olivier Girodet[1,2,3], Patrick Berger[1,2,3]

[1]Univ-Bordeaux, Centre de Recherche Cardio-thoracique de Bordeaux, U1045, Département de Pharmacologie, CIC 1401, F-33000 Bordeaux, France

[2]INSERM, Centre de Recherche Cardio-thoracique de Bordeaux, U1045, CIC 1401, F-33000 Bordeaux, France

[3]CHU de Bordeaux, Service d'exploration fonctionnelle respiratoire, Service de chirurgie thoracique, Service d'anatomopathologie, Service de radiologie, CIC 1401, F-33604 Pessac, France

* Equal contribution (co-1st author)

Corresponding author: Isabelle Dupin,

Univ-Bordeaux, Centre de Recherche Cardio-thoracique de Bordeaux, U1045, PTIB, Hôpital Xavier Arnozan, Avenue du Haut-Lévêque, F-33604 Pessac, France

Telephone number: +33 5 47 30 27 50 Fax number: +33 5 57 57 16 95

e-mail: isabelle.dupin@u-bordeaux.fr

Summary of the "take home" message

A high density of tissue fibrocytes is associated with reduced lung function and an increase in airway wall thickness.

Abstract

The remodelling mechanism and cellular players causing persistent airflow limitation in chronic obstructive pulmonary disease (COPD) remain largely elusive. We have recently demonstrated that circulating fibrocytes, a rare population of fibroblast-like cells produced by the bone marrow stroma, are increased in COPD patients during an exacerbation. We aimed to quantify fibrocyte density *in situ* in bronchial specimens from both control subjects and COPD patients, to define associations with relevant clinical, functional and computed tomography (CT) parameters and to investigate the effect of the epithelial microenvironment on fibrocyte survival *in vitro* ("Fibrochir" study).

A total of 17 COPD patients and 25 control subjects, all requiring thoracic surgery, were recruited. Using co-immunostaining and image analysis, we identified $CD45^+$ $FSP1^+$ cells as tissue fibrocytes and quantified their density in distal and proximal bronchial specimens. Fibrocytes, cultured from the blood samples of 6 COPD patients, were exposed to primary bronchial epithelial cell secretions from control subjects or COPD patients.

We demonstrate that fibrocytes are increased in both distal and proximal tissue specimens of COPD patients. The density of fibrocytes is negatively correlated with lung function parameters and positively correlated with bronchial wall thickness as assessed by CT scan. A high density of distal bronchial fibrocytes predicts the presence of COPD with a sensitivity of 83% and a specificity of 70%. Exposure of fibrocytes to COPD epithelial cell supernatant favours cell survival.

Our results thus demonstrate an increased density of fibrocytes within the bronchi of COPD patients, which may be promoted by epithelial-derived survival-mediating factors.

Key words: COPD, lung function, airway remodelling, CT scan, fibrocytes

Abbreviations

APC	Allophycocyanin
BEC	Bronchial Epithelial Cells
ColI	Collagen I
CSA	Cross Section Area
CSN	Cross Section Number
GOLD	Global Initiative for Chronic Obstructive Lung Disease
COPD	Chronic Obstructive Pulmonary Disease
CT	Computed Tomography
FEV_1	Forced Expiratory Volume in 1 Second
FITC	Fluorescein Isothiocyanate
FVC	Forced Vital Capacity
FSP1	Fibroblast-Specific Protein 1
LA	Lumen Area
LAA	Low Attenuation Area
MLA	Mean Lung Attenuation
$PaCO_2$	Arterial Partial Pressure of Carbon Dioxide
PaO_2	Arterial Partial Pressure of Oxygen
PE	Phycoerythrin
PBMC	Peripheral Blood Mononuclear Cells
α-SMA	α-smooth muscle actin
TLCO	Transfer Lung capacity of Carbon Monoxide
WA	Wall Area
WT	Wall Thickness

Introduction

Chronic obstructive pulmonary disease (COPD) is characterized by chronic persistent inflammation and remodelling leading to progressive airflow limitation [1, 2]. The evolution of this chronic disease is worsened by acute exacerbations, frequently triggered by viral or bacterial infections [3]. These exacerbations are considered an independent prognostic factor for mortality [4]. Current pharmacological treatments for COPD patients decrease exacerbation frequency by only up to 29% compared to placebo either alone or in combination, but they do not have any significant effect on mortality [5-9]. COPD patients exhibit remodelling processes leading to permanent changes in tissue structure, such as epithelial mucous metaplasia, parenchymal destruction (*i.e.*, emphysema) and connective-tissue deposition in the small airway walls [1]. The latter, also called peribronchiolar fibrosis, has been observed even in young smokers [10], thus suggesting that it may be an initiating event in COPD pathophysiology. These processes are not inhibited or reversed by current pharmacotherapy.

Fibrocytes are fibroblast-like cells produced by the bone marrow stroma and released in the peripheral circulation [11]. Circulating fibrocytes, defined as $CD45^+$ collagen I^+ cells, are increased in COPD patients only during an exacerbation [12] and not in a stable state compared to those in control subjects [12, 13]. A high blood fibrocyte concentration during an exacerbation is associated with an increased risk of death [12], suggesting a deleterious role of fibrocytes in COPD evolution. In contrast, myeloid-derived suppressor cell (MDSC)-like fibrocytes, a subpopulation of circulating fibrocytes, are increased in the blood of stable COPD patients, and these cells might play a protective role [13]. The presence and role of fibrocytes in the lungs of COPD patients remain controversial [13] and need to be clarified. Indeed, tissue fibrocytes, defined as $CD34^+$ collagen I^+ cells, have not been found in the distal airways of COPD patients and have been detected in the proximal airways of only less than 50% of COPD patients [13].

However, fibrocytes are known to downregulate CD34 expression when differentiating [14]. Thus, the co-expression of CD34 and collagen I, as a defining criterion for tissue fibrocytes, may lead to fibrocytes underestimation [13]. Therefore, we define fibrocytes as cells positive for both CD45 and fibroblast-specific protein 1 (FSP1), consistent with previous reports from human [15] and mouse [16-18] lungs.

Thus, the aim of the present study was to determine the density of tissue fibrocytes (*i.e.*, $CD45^+$ $FSP1^+$ cells) in distal and proximal airway specimens of COPD patients compared to that in control subjects. We then evaluated the relationship between the density of tissue fibrocytes and parameters derived from lung function tests and quantitative computed tomography (CT) as well as the relationship with blood fibrocytes. Functional *in vitro* experiments were also performed to assess the effect of the epithelial microenvironment on fibrocyte survival.

Methods

A more detailed description of the methods is provided in the online supplement.

Study populations

Subjects more than 40 years of age were eligible for enrolment if they required thoracic lobectomy surgery for cancer (pN0), lung transplantation or lung volume reduction (see Table E1 for individual indications). A total of 17 COPD patients with a clinical diagnosis of COPD according to the GOLD guidelines [2] and 25 non-COPD subjects ("control subjects") with normal lung function testing (*i.e.*, $FEV_1/FVC > 0.70$) and no chronic symptoms (cough or expectoration) were recruited from the University Hospital of Bordeaux.

To study fibrocytes *in vitro*, blood samples were obtained from a separate cohort of COPD patients, the COBRA cohort ("Cohorte Obstruction Bronchique et Asthme"; Bronchial

Obstruction and Asthma Cohort; sponsored by the French National Institute of Health and Medical Research, INSERM) (Tables E4 and E6).

Study design

This clinical trial was sponsored by the University Hospital of Bordeaux. The study was registered at ClinicalTrials.gov under the N° NCT01692444 (*i.e.*, "Fibrochir" study). The study protocol was approved by the local research ethics committee on May 30, 2012, and the French National Agency for Medicines and Health Products Safety on May 22, 2012. All subjects provided written informed consent. The study design is summarized in Fig E1. Four visits were scheduled: a pre-inclusion visit (V1) to explain the study and surgery, an inclusion visit (V2) on the day of the surgery, a visit one month ± 15 days after surgery (V3), and a final visit one year ± 15 days after surgery (V4).

Bronchial fibrocyte identification

A sub-segmental bronchus sample (for proximal tissue) and fragments of distal parenchyma were obtained from lung resection material at a distance from the tumour in the case of cancer. Additional proximal samples from the upper lobes and lower lobes were obtained from 4 transplant patients (patient numbers 48, 49, 51, and 52, see Table E1) to test potential differences in fibrocyte density in different lobes. The samples were embedded in paraffin, and 2.5 µm thick sections were cut and stained with a rabbit anti-FSP1 polyclonal antibody (Agilent, Les Ulis, France) and a mouse anti-CD45 monoclonal antibody (BD Biosciences, San Jose, CA), or a mouse anti-CD3 monoclonal antibody (Agilent), a mouse anti-CD19 monoclonal (Agilent), and a mouse anti-CD34 monoclonal antibody (Agilent). The sections were imaged using a Nanozoomer 2.0HT slide scanner (Hamamatsu Photonics, Massy, France). Quantification of FSP1 and CD45

double-positive cells was performed as described in Fig 1. The density of $FSP1^+$ $CD45^+$ cells was defined by the ratio between the numbers of double-positive cells in the lamina propria divided by the lamina propria area. Quantification of double-positive FSP1 and CD3, FSP1 and CD19 or FSP1 and CD34 cells was performed as described above with some modifications (see Supplemental Material and Methods in the online data supplement). Tissue area and cell measurements were all performed in a blinded fashion for patient characteristics.

Quantitative computed tomography

CT scans were performed on a Somatom Sensation Definition 64 (Siemens, Erlangen, Germany) at full inspiration and expiration and analysed using dedicated and validated software, as described previously [19-22]

Circulating fibrocyte identification

Non-adherent non-T (NANT) cells were purified from peripheral blood mononuclear cells (PBMCs) separated from the whole blood, and circulating fibrocytes were identified as cells double positive for the surface marker CD45 and the intracellular marker collagen I by flow cytometry, as described previously [12].

Bronchial epithelial supernatants

Human bronchial epithelial cells (BECs) were derived from bronchial specimens (see Table E5 for patient characteristics), as described previously [23]. Basal epithelial supernatant from fully differentiated epithelium was collected for further experiments.

Fibrocyte differentiation and survival

NANT cells purified from blood samples of COPD patients (Tables E4 and E6) were incubated for one week in DMEM (Fisher Scientific) supplemented with 20% foetal calf serum (Biowest, Riverside, USA), followed by another week in serum-free medium, or serum-free medium containing 50% basal epithelial supernatant. After 2 weeks in culture, the cells were fixed and stained for CD45, FSP1, fibronectin, vimentin, α-smooth muscle actin (α-SMA) and collagen I expression or detached by accutase (Fisher Scientific) and either fixed overnight with Cytofix/Cytoperm and stained to assess the expression of the same proteins or directly stained by propidium iodide (PI) to assess the percentage of dead cells (PI^+ cells) by flow cytometry.

Statistical analysis

Values are presented as the means ± SD or the medians (95% confidence interval [CI]). Statistical significance, defined as $P < 0.05$, was analysed by Fisher's exact test for the comparison of proportions, by two-sided independent t-test for variables with a parametric distribution, and by Wilcoxon test, Mann–Whitney U test and Spearman's correlation coefficient for variables with a non-parametric distribution. Concerning correlation analyses, no mathematical correction was made for multiple comparisons, as previously recommended [24]. A receiver operating characteristic (ROC) analysis and a univariate logistic regression analysis were performed to evaluate the association between COPD and a high density of tissue fibrocytes.

Results

Study population

The number of patients enrolled, excluded or followed for up to 1 year after surgery is shown in supplemental Fig E1. Clinical and functional characteristics, as well as quantitative CT parameters of all subjects with tissue fibrocyte assessment, are shown in Table 1. The groups of control and COPD patients were well matched for age and body mass index. As expected, COPD patients were significantly different from controls in terms of smoking habits, lung function (FEV_1, FVC, FEV_1/FVC ratio, and RV), diffusing capacity (TLCO) and CT parameters, including wall thickness, emphysema extent (LAA), air trapping (MLA E) and cross-sectional pulmonary vessel area and number (CSA, CSN) (Table 1). The sex ratio was also different with more men in the COPD group.

Bronchial fibrocytes numbers are increased in COPD patients

As a methodological control, we first cultured fibrocytes from blood samples from a separate cohort of COPD patients (Table E4), and we showed that virtually all $CD45^+$ $FSP1^+$ cells (99.7 ± 0.5%, n=9) purified from circulating PBMCs also express collagen I (colI) after 14 days of differentiation *in vitro* (Fig E2). Similarly, 87.5 ± 6.2% of $CD45^+$ collagen I^+ cells were positive for FSP1 staining in the same culture conditions (n=9). $CD45^+$ $FSP1^+$ cells spontaneously express mesenchymal cell markers, such as vimentin (99.9 ± 0.1%, n=6), fibronectin (73.3 ± 0.1%, n=2), and α-SMA (100 ± 0%, n=6) (Fig E2). This allows us to define tissue fibrocytes as $CD45^+$ $FSP1^+$ cells. These cells were identified by immunohistochemistry as shown in Fig 1, and they were detected in distal tissue specimens from 11 of 12 COPD patients (92%) and 13 of 20 control subjects (65%) (Fig 2) as well as in proximal tissue specimens from 14 of 14 COPD patients (100%) and 16 of 21 control subjects (76%) (Fig 3).

These fibrocytes were located in the sub-epithelial region of both distal and proximal airways (Figs 2a and 3a) and, occasionally, within the epithelial layer. No $CD45^+$ $FSP1^+$ cells were evident within the airway smooth muscle layer. Some tissue fibrocytes were found in the peribronchial area outside the smooth muscle layer (Fig E3). However, the analysis of fibrocyte density in this latter region could not be performed systematically since this area could not be identified in each of our tissue specimens. The density of bronchial fibrocytes was higher in the sub-epithelial region of distal airways of COPD patients (median = 133 cells/μm^2 (95% CI, 40 to 469), n = 12) than in that of control subjects (median = 42 cells/μm^2 (95% CI, 31 to 114), n = 20, $P<0.05$) (Fig 2b). Similarly, fibrocyte density was also increased in the proximal airways of COPD patients (median = 73 cells/μm^2 (95% CI, 47 to 139), n = 14) compared with those of control subjects (median = 21 cells/μm^2 (95% CI, 18 to 60), n = 21, $P<0.05$) (Fig 3b). In both distal and proximal airways, there was no difference in sub-epithelial areas considered for tissue fibrocyte quantification between COPD patients and control subjects (Figs 2c and 3c). Not surprisingly, however, the density of fibrocytes in the sub-epithelial area of the proximal tissue was positively and significantly correlated with that measured in the distal airways (Fig E4). Since COPD has been described as a heterogeneous upper lobe predominant disease in subgroups of patients [2], we wondered whether fibrocytes specifically accumulated in the upper lobes. For distal and proximal tissue specimens, there was no significant difference in fibrocyte density between these two sites (Fig E5a-b). Taking advantage of the various localization of sample sites from transplant patients (n = 4), we also observed that fibrocyte density was not significantly different from upper to lower lobes in these patients (Fig E5c). In both proximal and distal specimens, fibrocyte density remained significantly increased in COPD patients compared to control smokers when the never smoked control subjects were removed from the analysis (Fig E6). To account for the sex differences between COPD patients and control subjects, we

performed another subgroup analysis in sex- and age-matched patients. Consequently, the sex ratios were identical (50% in both subgroups). Fibrocyte density in the proximal, but not distal, tissue remained significantly higher in COPD patients than matched control subjects (Fig E7a-b).

To further confirm our results, we co-stained FSP1 with CD3 or CD19 to determine whether FSP1-positive cells could be T lymphocytes or B lymphocytes, respectively. Except for one control subject, very few $CD3^+$ cells also expressed FSP1 (Fig E8a), and there was no significant difference in the density of $CD3^+$ $FSP1^+$ cells in the sub-epithelial region of the distal airways between controls and COPD patients (Fig E8b-c). Similarly, this density in the proximal airways was not significantly different between the groups (Fig E8d-e). The B lymphocyte CD19 marker co-localized with FSP1-positive cells neither in distal (Fig E9a) nor in proximal (Fig E9b) tissue specimens. We also co-immunostained CD34 and FSP1. $CD34^+$ $FSP1^+$ cells were detected in distal tissue specimens from only 2 of 12 COPD patients (17%) and 4 of 20 control subjects (20%) (Fig E10). $CD34^+$ $FSP1^+$ cells were found in proximal tissue specimens from 9 of 13 COPD patients (69%) and 11 of 21 control subjects (52%) (Fig E11), but the density of these cells in COPD patients (median = 0.5 cells/μm^2 (95% CI, 0.1 to 1.7), n = 13) was very low compared with that of $CD45^+$ $FSP1^+$ cells (median = 73 cells/μm^2 (95% CI, 47 to 139), n=14) (Fig 2b). In both distal and proximal airways, there was no difference in the density of $CD34^+$ $FSP1^+$ cells between COPD patients and control subjects (Figs E10 and E11).

Relationships between bronchial fibrocyte density and functional and CT parameters

We determined the univariate correlation coefficients between the density of tissue fibrocytes in the sub-epithelial region of both distal and proximal airways and various functional and CT parameters, without correcting for multiple testing (Tables E2 and E3). In the distal tissue specimens, the density of fibrocytes was negatively correlated with the FEV_1/FVC ratio (Fig 4a)

and positively correlated with $PaCO_2$ (Fig 4b). The density of tissue fibrocytes was also significantly associated with the mean lung attenuation value during exhalation (Fig 4c). In the proximal tissue specimens, the density of fibrocytes was negatively correlated with FEV_1 (Fig 4d) and FVC (Table E2) and positively correlated with RV (Table E2), WT4 (Fig 4e), WT5 (Fig 4f), and WA4% (Table E2). Moreover, we observed identical key correlations when the never smoked control subjects were removed from the analysis (Fig E12). Again, considering sex differences between COPD patients and control subjects, we determined key correlations coefficients in a subgroup analysis of sex- and age-matched patients. All key correlations previously found in the whole population remained significant, except for the relationship between distal fibrocyte density and $PaCO_2$ (Fig E7c-h).

Receiver operator characteristic (ROC) curves were built for all subjects whose density of tissue fibrocytes was assessed in distal (n=12 COPD patients and 20 control subjects, Fig 5a) and proximal (n=14 COPD patients and 21 control subjects, Fig 5b) tissue specimens with significant areas under the curves (Table 2). To predict COPD, the density of fibrocytes in the distal airways had a sensitivity of 83% and a specificity of 70%, whereas this density had a sensitivity of 79% and a specificity of 67% in the proximal airways (Table 2). Moreover, the negative predictive value to eliminate COPD was 97.5% and 96.6% for the distal and proximal airways, respectively, using a prevalence of 10% for COPD in the general population [25]. ROC analyses allowed us to select the optimal value of fibrocyte density (cut-off values of 72 and 32 for distal and proximal tissue, respectively) to classify patients either with a high or low level of tissue fibrocytes (Table 2). COPD was associated with a high density of fibrocytes in distal (odds ratio: 11.7; 95% CI: [1.9-70.2]; $P < 0.05$) and proximal (odds ratio: 7.3; 95% CI: [1.5-35.1]; $P < 0.05$) airways. Thus, a high tissue fibrocyte density is associated with an increased risk of COPD.

Circulating fibrocytes are unchanged in stable COPD

The percentage of blood fibrocytes ($CD45^+$ $ColI^+$ cells) in PBMCs was not significantly different between stable COPD patients (median=10.3% (95% CI, 4.6 to 16.5) of PBMCs, n=12) and control subjects (median=7.9% (95% CI, 4.1 to 11.6) of PBMCs, n=22) (Fig E13a). A similar result was obtained when the fibrocyte concentration was expressed as absolute counts per millilitre of blood (data not shown). Finally, the percentage of blood fibrocytes (*i.e.*, $CD45^+$ $ColI^+$ cells) in PBMCs was significantly correlated with the density of bronchial fibrocytes (*i.e.*, $CD45^+$ $FSP1^+$ cells) in the distal airways (Fig E13b).

COPD epithelial supernatant favours fibrocyte survival

We next investigated whether secretions from bronchial epithelial cells (BECs) from control or COPD patients could affect fibrocyte viability in an *in vitro* assay. We evaluated this effect using BECs obtained from lung resection material sampled either in control subjects (n=2) or in COPD patients (n=2) (Table E5), cultured at the air-liquid interface. Fibrocytes were cultured from blood samples from a separate cohort of 6 COPD patients (Table E6). Seven to ten days after blood sampling, cells, almost all of which were $CD45^+$ $FSP1^+$ (94.9 ± 3.6%), were exposed for 7 days to a mixture of fully differentiated BEC supernatants derived either from control subjects or COPD patients. Seven days after initial exposure, the level of $CD45^+$ $FSP1^+$ cells remained high (92.9 ± 3.9% and 93.4 ± 3.3%, for the control and COPD conditions, respectively). However, exposure of fibrocytes to COPD epithelial supernatant significantly decreased the percentage of dying cells (Fig E14).

Discussion

In the present study, we have shown that the density of tissue fibrocytes (*i.e.*, $CD45^+$ $FSP1^+$ cells) is significantly greater in both distal and proximal airway specimens of COPD patients compared to that of control subjects. We also found a significant correlation between this tissue fibrocyte density and blood fibrocytes as well as airway obstruction, increased wall thickness, or air trapping. Using ROC curve analysis and univariate logistic regression analysis, we observed that a high density of tissue fibrocytes increases the likelihood of COPD. Finally, it appears that fibrocyte survival is increased by epithelial cell secretions from COPD patients, a mechanism that could contribute to the elevated sub-epithelial density of fibrocytes in COPD patients.

There is a discrepancy between the present results and those previously obtained by Wright and colleagues [13], which deserves some methodological discussion. Wright *et al* did not find an increased level of tissue fibrocytes in COPD patients. They did not even observe any fibrocytes in distal airways [13]. However, the methodology of tissue fibrocyte assessment and, ultimately, the definition of fibrocytes are different in the present study and in that of Wright *et al* [13]. Wright and colleagues' method relied on the identification of CD34 and collagen I staining on sequential, instead of identical, sections [13], which could lead to either false fibrocyte identification because of apparent co-expression in closely apposed but not identical cells or fibrocyte underestimation because of the absence of co-expression in cells that are present only in one section. We have carefully addressed this issue by using antibodies and chromogens that are compatible with co-immunostaining in the same section. We have thus developed an image analysis technique that unambiguously identifies fibrocytes. Moreover, defining tissue fibrocytes as $CD34^+$ collagen I^+ cells [13] may lead to fibrocyte underestimation, which is consistent with previous data showing a downregulation of CD34 expression when fibrocytes differentiate in

culture [14]. In regard to the connection, the present data confirming the very low density of $CD34^+$ $FSP1^+$ cells in bronchial specimens are thus consistent with those of Wright *et al*. Fibrocytes are commonly defined as cells co-expressing CD45 and collagen I [26]. The expression of a haematopoietic marker, such as CD45, is one of the minimum criteria for fibrocyte identification [26] and was used in the present study. However, since immunohistochemistry for collagen I failed to unambiguously identify collagen I^+ cells in our experiments (data not shown), as well as in another report [27]; therefore, we used the FSP1 marker as a co-marker with CD45 for fibrocyte identification, as previously extensively described [15-18]. FSP1 [28], also known as S100A4, is used as a marker for lung fibroblasts [27]. Most pulmonary $FSP1^+$ cells express collagen I [27, 29], and the number of $FSP1^+$ cells correlates with the extent of lung fibrosis in a murine model of fibrosis, suggesting that these cells contribute to collagen deposition [27]. In addition, we have shown that almost all the $CD45^+$ $FSP1^+$ cells purified from circulating PBMCs also express collagen I, as well as mesenchymal cell markers, such as vimentin, fibronectin and α-SMA, after 14 days of differentiation *in vitro* (Fig E2), which is consistent with the definition of fibrocyte as a myofibroblast precursor as previously described [11, 14, 30]. It thus appears that the term tissue fibrocyte is more accurate for CD45 and FSP1 double-positive cells. Since FSP1 expression was initially identified in fibroblasts [28] but was subsequently characterized in immune cells such as T and B lymphocytes [15], we paid special attention to co-immunostaining of FSP1 with CD3 or CD19. In doing so, we showed that T lymphocytes co-expressing CD3 and FSP1 represented only a minor subset of $CD45^+$ $FSP1^+$ cells, the density of which did not change in COPD patients. We also showed that no B lymphocytes co-expressing CD19 and FSP1 were present in either distal or proximal human bronchi from both control subjects and COPD patients. Finally, FSP1 expression has also been characterized in macrophages [29]. However, numerous macrophage markers, such as CD68,

CD163, CD204, CD206, and CD209, are also expressed by fibrocytes [31-33]. It is thus impossible to properly differentiate fibrocytes from macrophages using immunohistochemistry even if collagen I^+ $CD45^+$ double-staining was suitable.

Our results may support a potential role for tissue fibrocytes in COPD. Indeed, the greater the density of bronchial fibrocytes is, the lower the FEV1 value or the FEV1/FVC ratio. Similarly, the greater the density of bronchial fibrocytes is, the greater the bronchial wall thickness or the pulmonary air trapping. Although the association between fibrocyte presence and the alteration of lung function combined with anatomical modifications suggests a deleterious effect of fibrocytes, we would like to emphasize that the association does not demonstrate that these cells play a causative role herein. We previously pointed out a potential detrimental role of blood fibrocytes, since a high concentration of fibrocytes in the peripheral circulation of COPD patients during an acute exacerbation was associated with a higher mortality [12]. Moreover, blood fibrocytes were present at a high level in frequent exacerbating patients [12]. Since small airways are the major site of airway obstruction in COPD [34-37], the observation that tissue fibrocyte density, assessed in the present study, was higher in distal than in proximal airways makes sense. The correlation between the concentration of circulating fibrocytes and the density of distal bronchial fibrocytes may indicate that fibrocytes, which are recruited in the blood during an acute exacerbation [12], subsequently migrate to the airways and could participate in the tissue repair and remodelling processes. Indeed, once recruited to the lungs, fibrocytes may play various roles, including matrix secretion and degradation, pro-fibrotic cytokine production and activation of contractile force [38]. The presence of fibrocytes in the lungs of patients affected with asthma [14, 39, 40] and idiopathic pulmonary fibrosis [41] suggests a physiological repair response in several types of lung damage. On the one hand, this repair process should spontaneously resolve with time and

should disappear with tobacco smoking cessation. On the other hand, a switch to aberrant repair or to excessive degradation may participate in abnormal remodelling processes, such as peribronchial fibrosis and emphysema. The reduced cell death in fibrocytes cultured with BECs from COPD patients, detected by the single PI-positive method, combined with the elevated density of fibrocytes at the proximity of the epithelium in tissue samples from COPD patients, suggests that secretions from epithelial cells in the COPD microenvironment provides pro-survival signals for tissue fibrocytes and could explain, at least partially, the bronchial accumulation of fibrocytes in COPD patients. Whether fibrocyte persistence in COPD patients participates to aberrant repair processes and chronic inflammation is still under investigation. The specific role of fibrocytes in COPD pathogenesis remains another open question. Specific physical and chemical signals originating from the microenvironment are likely to play a key role in regulating fibrocyte final localization, differentiation and function inside the tissue [38].

In light of the important gender differences observed in COPD patients [42], as well as in COPD mouse models [43], we tested whether our results reflect sex differences. Matching the patients by sex suggested that our results are not related to gender-related features. The question of fibrocytes participation in sex-related differences in the clinical expression of COPD between men and women remains to be properly addressed in future studies that are appropriately powered for gender analysis.

The present study has some limitations, which deserve further comments. Additional studies are required to explore the cellular and molecular mechanisms involved in epithelium-dependent fibrocyte survival. Continuous efforts are warranted to clarify the cellular mechanisms by which fibrocytes participate in obstruction development. The specimens for fibrocyte detection were obtained from patients with a diagnosis of lung cancer in 37 of 42 patients. As FSP1 is often expressed in malignant cells [44, 45], one may suggest that it could have an impact on the

fibrocyte density measured in our study. Since (i) bronchial specimens for fibrocyte analysis were selected from macroscopically normal lung resection material and (ii) patients with a staging different from pN0 confirmed after surgery were excluded, it is unlikely that malignancy was sufficient to explain the increase in fibrocyte density we observed in COPD patients.

In conclusion, by taking advantage of unambiguous fibrocyte identification by co-immunostaining and image analysis, we unveil that COPD patients exhibit a greater density of fibrocytes in distal and proximal airways than control subjects. A high density of tissue fibrocytes is associated with lower lung function, airway structural changes and a higher risk of COPD, underlying the need for further studies to investigate the physiological and pathophysiological functions of fibrocytes.

Acknowledgements

The authors thank the study participants, the staff of Thoracic Surgery, Radiology, Pathology, Respiratory and Lung Function Testing departments from the University Hospital of Bordeaux, Virginie Niel for technical assistance, and the Bordeaux Imaging Center (BIC) for help with imaging and image analysis. Microscopy was performed at the Bordeaux Imaging Center, a service unit of the CNRS-INSERM and Bordeaux University, a member of the national BioImaging infrastructure of France supported by the French National Research Agency (ANR-10-INBS-04). The help of Christel Poujol, Sébastien Marais and Fabrice Cordelières for imaging, the help of Muriel Cario-André for immunohistochemistry and the help of Pierre Vallois for statistics are acknowledged.

Funding:

This study was sponsored and supported by Bordeaux University Hospital (*i.e.,* "CHU de Bordeaux"). This study was supported by a grant from the "Fondation Bordeaux Université," with funding from "Assistance Ventilatoire à Domicile" (AVAD) and "Fédération Girondine de Lutte contre les Maladies Respiratoires" (FGLMR).

References

1. Hogg JC, Chu F, Utokaparch S, Woods R, Elliott WM, Buzatu L, Cherniack RM, Rogers RM, Sciurba FC, Coxson HO, Pare PD. The nature of small-airway obstruction in chronic obstructive pulmonary disease. *N Engl J Med* 2004: 350(26): 2645-2653.
2. GOLD 1998. Global Initiative for Chronic Obstructive Lung Disease. Global Strategy for the Diagnosis, Management and Prevention of Chronic Obstructive Pulmonary Disease. NIH Publication (updated 2019). Accessed January 1, 2019, at http://www.goldcopd.org.
3. Ko FW, Chan KP, Hui DS, Goddard JR, Shaw JG, Reid DW, Yang IA. Acute exacerbation of COPD. *Respirology* 2016: 21(7): 1152-1165.
4. Soler-Cataluna JJ, Martinez-Garcia MA, Roman Sanchez P, Salcedo E, Navarro M, Ochando R. Severe acute exacerbations and mortality in patients with chronic obstructive pulmonary disease. *Thorax* 2005: 60(11): 925-931.
5. Calverley PM, Anderson JA, Celli B, Ferguson GT, Jenkins C, Jones PW, Yates JC, Vestbo J. Salmeterol and fluticasone propionate and survival in chronic obstructive pulmonary disease. *N Engl J Med* 2007: 356(8): 775-789.
6. Tashkin D, Celli B, Senn S, Burkhart D, Kesten S, Menjoge S, Decramer M. A 4-year trial of tiotropium in chronic obstructive pulmonary disease (UPLIFT trial). *Rev Port Pneumol* 2009: 15(1): 137-140.
7. Vestbo J, Anderson JA, Brook RD, Calverley PM, Celli BR, Crim C, Martinez F, Yates J, Newby DE, Investigators S. Fluticasone furoate and vilanterol and survival in chronic obstructive pulmonary disease with heightened cardiovascular risk (SUMMIT): a double-blind randomised controlled trial. *Lancet* 2016: 387(10030): 1817-1826.
8. Wedzicha JA, Banerji D, Chapman KR, Vestbo J, Roche N, Ayers RT, Thach C, Fogel R, Patalano F, Vogelmeier CF, Investigators F. Indacaterol-Glycopyrronium versus Salmeterol-Fluticasone for COPD. *N Engl J Med* 2016: 374(23): 2222-2234.
9. Lipson DA, Barnhart F, Brealey N, Brooks J, Criner GJ, Day NC, Dransfield MT, Halpin DMG, Han MK, Jones CE, Kilbride S, Lange P, Lomas DA, Martinez FJ, Singh D, Tabberer M, Wise RA, Pascoe SJ, Investigators I. Once-Daily Single-Inhaler Triple versus Dual Therapy in Patients with COPD. *N Engl J Med* 2018: 378(18): 1671-1680.
10. Niewoehner DE, Kleinerman J, Rice DB. Pathologic changes in the peripheral airways of young cigarette smokers. *N Engl J Med* 1974: 291(15): 755-758.
11. Bucala R, Spiegel LA, Chesney J, Hogan M, Cerami A. Circulating fibrocytes define a new leukocyte subpopulation that mediates tissue repair. *Mol Med* 1994: 1(1): 71-81.
12. Dupin I, Allard B, Ozier A, Maurat E, Ousova O, Delbrel E, Trian T, Bui HN, Dromer C, Guisset O, Blanchard E, Hilbert G, Vargas F, Thumerel M, Marthan R, Girodet PO, Berger P. Blood fibrocytes are recruited during acute exacerbations of chronic obstructive pulmonary disease through a CXCR4-dependent pathway. *J Allergy Clin Immunol* 2016: 137(4): 1036-1042 e1037.
13. Wright AK, Newby C, Hartley RA, Mistry V, Gupta S, Berair R, Roach KM, Saunders R, Thornton T, Shelley M, Edwards K, Barker B, Brightling CE. Myeloid-derived suppressor cell-like fibrocytes are increased and associated with preserved lung function in chronic obstructive pulmonary disease. *Allergy* 2017: 72(4): 645-655.
14. Schmidt M, Sun G, Stacey MA, Mori L, Mattoli S. Identification of circulating fibrocytes as precursors of bronchial myofibroblasts in asthma. *J Immunol* 2003: 171(1): 380-389.
15. Mitsuhashi A, Goto H, Saijo A, Trung VT, Aono Y, Ogino H, Kuramoto T, Tabata S, Uehara H, Izumi K, Yoshida M, Kobayashi H, Takahashi H, Gotoh M, Kakiuchi S, Hanibuchi M, Yano S, Yokomise H, Sakiyama S, Nishioka Y. Fibrocyte-like cells mediate acquired resistance to anti-angiogenic therapy with bevacizumab. *Nat Commun* 2015: 6: 8792.

16. Sangaletti S, Tripodo C, Cappetti B, Casalini P, Chiodoni C, Piconese S, Santangelo A, Parenza M, Arioli I, Miotti S, Colombo MP. SPARC oppositely regulates inflammation and fibrosis in bleomycin-induced lung damage. *Am J Pathol* 2011: 179(6): 3000-3010.
17. Rock JR, Barkauskas CE, Cronce MJ, Xue Y, Harris JR, Liang J, Noble PW, Hogan BL. Multiple stromal populations contribute to pulmonary fibrosis without evidence for epithelial to mesenchymal transition. *Proc Natl Acad Sci U S A* 2011: 108(52): E1475-1483.
18. Aono Y, Kishi M, Yokota Y, Azuma M, Kinoshita K, Takezaki A, Sato S, Kawano H, Kishi J, Goto H, Uehara H, Izumi K, Nishioka Y. Role of platelet-derived growth factor/platelet-derived growth factor receptor axis in the trafficking of circulating fibrocytes in pulmonary fibrosis. *Am J Respir Cell Mol Biol* 2014: 51(6): 793-801.
19. Coste F, Dournes G, Dromer C, Blanchard E, Freund-Michel V, Girodet PO, Montaudon M, Baldacci F, Picard F, Marthan R, Berger P, Laurent F. CT evaluation of small pulmonary vessels area in patients with COPD with severe pulmonary hypertension. *Thorax* 2016: 71(9): 830-837.
20. Dournes G, Laurent F, Coste F, Dromer C, Blanchard E, Picard F, Baldacci F, Montaudon M, Girodet PO, Marthan R, Berger P. Computed tomographic measurement of airway remodeling and emphysema in advanced chronic obstructive pulmonary disease. Correlation with pulmonary hypertension. *Am J Respir Crit Care Med* 2015: 191(1): 63-70.
21. Girodet PO, Dournes G, Thumerel M, Begueret H, Dos Santos P, Ozier A, Dupin I, Trian T, Montaudon M, Laurent F, Marthan R, Berger P. Calcium Channel Blocker Reduces Airway Remodeling in Severe Asthma. A Proof-of-Concept Study. *Am J Respir Crit Care Med* 2015: 191(8): 876-883.
22. Montaudon M, Berger P, de Dietrich G, Braquelaire A, Marthan R, Tunon-de-Lara JM, Laurent F. Assessment of airways with three-dimensional quantitative thin-section CT: in vitro and in vivo validation. *Radiology* 2007: 242(2): 563-572.
23. Trian T, Allard B, Dupin I, Carvalho G, Ousova O, Maurat E, Bataille J, Thumerel M, Begueret H, Girodet PO, Marthan R, Berger P. House dust mites induce proliferation of severe asthmatic smooth muscle cells via an epithelium-dependent pathway. *Am J Respir Crit Care Med* 2015: 191(5): 538-546.
24. Rothman KJ. No adjustments are needed for multiple comparisons. *Epidemiology* 1990: 1(1): 43-46.
25. Halbert RJ, Natoli JL, Gano A, Badamgarav E, Buist AS, Mannino DM. Global burden of COPD: systematic review and meta-analysis. *Eur Respir J* 2006: 28(3): 523-532.
26. Reilkoff RA, Bucala R, Herzog EL. Fibrocytes: emerging effector cells in chronic inflammation. *Nat Rev Immunol* 2011: 11(6): 427-435.
27. Lawson WE, Polosukhin VV, Zoia O, Stathopoulos GT, Han W, Plieth D, Loyd JE, Neilson EG, Blackwell TS. Characterization of fibroblast-specific protein 1 in pulmonary fibrosis. *Am J Respir Crit Care Med* 2005: 171(8): 899-907.
28. Strutz F, Okada H, Lo CW, Danoff T, Carone RL, Tomaszewski JE, Neilson EG. Identification and characterization of a fibroblast marker: FSP1. *J Cell Biol* 1995: 130(2): 393-405.
29. Inoue T, Plieth D, Venkov CD, Xu C, Neilson EG. Antibodies against macrophages that overlap in specificity with fibroblasts. *Kidney Int* 2005: 67(6): 2488-2493.
30. Phillips RJ, Burdick MD, Hong K, Lutz MA, Murray LA, Xue YY, Belperio JA, Keane MP, Strieter RM. Circulating fibrocytes traffic to the lungs in response to CXCL12 and mediate fibrosis. *J Clin Invest* 2004: 114(3): 438-446.
31. Hu X, DeBiasi EM, Herzog EL. Flow Cytometric Identification of Fibrocytes in the Human Circulation. *Methods Mol Biol* 2015: 1343: 19-33.
32. Pilling D, Fan T, Huang D, Kaul B, Gomer RH. Identification of markers that distinguish monocyte-derived fibrocytes from monocytes, macrophages, and fibroblasts. *PLoS One* 2009: 4(10): e7475.
33. Bianchetti L, Barczyk M, Cardoso J, Schmidt M, Bellini A, Mattoli S. Extracellular matrix remodelling properties of human fibrocytes. *J Cell Mol Med* 2012: 16(3): 483-495.
34. Hogg JC, Macklem PT, Thurlbeck WM. Site and nature of airway obstruction in chronic obstructive lung disease. *N Engl J Med* 1968: 278(25): 1355-1360.

35. Hasegawa M, Nasuhara Y, Onodera Y, Makita H, Nagai K, Fuke S, Ito Y, Betsuyaku T, Nishimura M. Airflow limitation and airway dimensions in chronic obstructive pulmonary disease. *Am J Respir Crit Care Med* 2006: 173(12): 1309-1315.
36. Hogg JC, McDonough JE, Suzuki M. Small airway obstruction in COPD: new insights based on micro-CT imaging and MRI imaging. *Chest* 2013: 143(5): 1436-1443.
37. Hogg JC, Pare PD, Hackett TL. The Contribution of Small Airway Obstruction to the Pathogenesis of Chronic Obstructive Pulmonary Disease. *Physiol Rev* 2017: 97(2): 529-552.
38. Dupin I, Contin-Bordes C, Berger P. Fibrocytes in Asthma and Chronic Obstructive Pulmonary Disease: Variations on the Same Theme. *Am J Respir Cell Mol Biol* 2018: 58(3): 288-298.
39. Nihlberg K, Larsen K, Hultgardh-Nilsson A, Malmstrom A, Bjermer L, Westergren-Thorsson G. Tissue fibrocytes in patients with mild asthma: a possible link to thickness of reticular basement membrane? *Respir Res* 2006: 7: 50.
40. Saunders R, Siddiqui S, Kaur D, Doe C, Sutcliffe A, Hollins F, Bradding P, Wardlaw A, Brightling CE. Fibrocyte localization to the airway smooth muscle is a feature of asthma. *J Allergy Clin Immunol* 2009: 123(2): 376-384.
41. Heukels P, van Hulst JAC, van Nimwegen M, Boorsma CE, Melgert BN, van den Toorn LM, Boomars KAT, Wijsenbeek MS, Hoogsteden H, von der Thusen JH, Hendriks RW, Kool M, van den Blink B. Fibrocytes are increased in lung and peripheral blood of patients with idiopathic pulmonary fibrosis. *Respir Res* 2018: 19(1): 90.
42. Jenkins CR, Chapman KR, Donohue JF, Roche N, Tsiligianni I, Han MK. Improving the Management of COPD in Women. *Chest* 2017: 151(3): 686-696.
43. Tam A, Churg A, Wright JL, Zhou S, Kirby M, Coxson HO, Lam S, Man SF, Sin DD. Sex Differences in Airway Remodeling in a Mouse Model of Chronic Obstructive Pulmonary Disease. *Am J Respir Crit Care Med* 2016: 193(8): 825-834.
44. Ilg EC, Schafer BW, Heizmann CW. Expression pattern of S100 calcium-binding proteins in human tumors. *Int J Cancer* 1996: 68(3): 325-332.
45. Xue C, Plieth D, Venkov C, Xu C, Neilson EG. The gatekeeper effect of epithelial-mesenchymal transition regulates the frequency of breast cancer metastasis. *Cancer Res* 2003: 63(12): 3386-3394.

Fig legends

Fig 1. Detection of $CD45^+$ $FSP1^+$ cells.

a, Left column, CD45 (green) and fibroblast-specific protein 1 (FSP1, red) staining. Middle column, images for CD45 (top panel) and FSP1 (bottom panel) staining obtained after colour deconvolution. Right column, segmented images obtained for CD45 (top panel) and FSP1 staining (bottom panel) after segmentation by a binary threshold. b, Merged segmented image. c, Higher magnification of the segmented image in b. The yellow arrowheads and the white arrows indicate $CD45^+$ $FSP1^+$ cells and $CD45^+$ cells, respectively.

Fig 2. Increased fibrocyte density in distal airways of COPD patients.

a, Representative staining of CD45 (green) and FSP1 (red) in distal bronchial tissue specimens from a control subject (left) and a COPD patient (right). The yellow arrowheads indicate fibrocytes, defined as $CD45^+$ $FSP1^+$ cells. b, Quantification of fibrocyte density (normalized by the sub-epithelial area) in one specimen/patient. *: $P<0.05$, Mann-Whitney test. c, Comparison of the sub-epithelial areas in control subjects and COPD patients. b, c, The medians are represented as horizontal lines.

Fig 3. Increased fibrocyte density in the proximal airways of COPD patients.

a, Representative staining of CD45 (green) and FSP1 (red) in proximal bronchial tissue specimens from a control subject (left) and a COPD patient (right). The yellow arrowheads indicate fibrocytes, defined as $CD45^+$ $FSP1^+$ cells. b, Quantification of fibrocyte density (normalized by the sub-epithelial area) in one specimen/patient. *: $P<0.05$, Mann-Whitney test. c,

Comparison of the sub-epithelial areas in control subjects and COPD patients. b, c, The medians are represented as horizontal lines.

Fig 4. Relationships between fibrocyte density, lung function parameters and CT parameters.

a-c, Relationships between FEV1/FVC (a), PaO_2 (b), MLA during expiration (c) and the density of $CD45^+$ $FSP1^+$ cells in distal airways measured in control subjects (black circles) and COPD patients (open circles). d-f, Relationships between FEV1 (d), WT4 (e), WT5 (f) and the density of $CD45^+$

$FSP1^+$ cells in proximal airways measured in control subjects (black circles) and COPD patients (open circles). The correlation coefficient (r) and significance level (P value) were obtained by using nonparametric Spearman analysis.

Fig 5. Diagnosis accuracy of high fibrocyte density for COPD

a-b, Receiver operating characteristic (ROC) curves for control subjects and COPD patients with fibrocyte density measured in distal (a) or proximal (b) tissue specimens–were built to predict COPD.

Table 1: Patient characteristics

	COPD	Control	P value
n	17	25	
Age (yrs.)	66.2 ± 9.5	61.7 ± 8.1	0.11
Sex (Male/Female)	11/6	5/20	0.008
Body-mass index (kg/m^2)	24.7 ± 4.1	26.5 ± 6.9	0.34
Current smoker (Y/N)	2/15	10/15	0.09
Former smoker (Y/N)	15/2	8/17	0.0004
Pack years (no.)	43.7 ± 22.8	18.1 ± 16.8	0.0007
LFT			
FEV_1 (% pred.)	57.2 ± 22.5	100.0 ± 16.7	<0.0001
FEV_1/FVC ratio (%)	53.2 ± 16.3	78.0 ± 8.0	<0.0001
FVC (% pred.)	82.0 ± 15.4	107 ± 15.8	<0.0001
RV (% pred.)	168 ± 68.8	112 ± 27.8	0.0007
TLCO (% pred.)	53.4 ± 22.6	81.8 ± 20.4	0.0003
Six-minute walk test distance (m)	472 ± 67	503 ± 69	0.19
Arterial blood gases			
PaO_2 (mm Hg)	78.0 ± 11.2	85.1 ± 13.2	0.08
$PaCO_2$ (mm Hg)	40.7 ± 7.7	35.7 ± 2.8	0.01
CT parameters			
Bronchi:			
WA4%	4.2 ± 0.4	3.8 ± 0.6	0.06
WT4 (mm)	1.7 ± 0.2	1.5 ± 0.2	0.03
WA5%	4.2 ± 0.4	3.2 ± 0.4	<0.0001
WT5 (mm)	1.5 ± 0.2	1.3 ± 0.2	0.02
Emphysema:			
LAA (%)	21.9 ± 16.6	4.2 ± 4.0	<0.0001
Emphysema (Y/N)	12/5	3/22	0.0002
Air trapping:			
MLA E (HU)	-858 ± 23	-817 ± 38	0.002
MLA I (HU)	-865 ± 24	- 821 ± 33	0.0001
MLA I-E (HU)	-7.5 ± 12	-7.7 ± 31	0.52
Pulmonary vessels:			
$\%CSA_{<5}$	0.35 ± 0.10	0.54 ± 0.20	0.0003
$\%CSA_{5-10}$	0.11 ± 0.02	0.15 ± 0.04	0.0008
$CSN_{<5}$	0.28 ± 0.03	0.47 ± 0.19	0.0004
CSN_{5-10}	0.016 ± 0.004	0.023 ± 0.006	0.0008

Plus–minus values indicate means ± SD. LFT, lung function test; FEV_1, forced expiratory volume in 1 second; FVC, forced vital capacity; RV, residual volume; TLCO, transfer lung capacity of carbon monoxide, PaO_2, partial arterial oxygen pressure, $PaCO_2$, partial arterial carbon dioxide pressure; WA, mean wall area; LA, mean lumen area, WA%, mean wall area percentage; WT, wall thickness; LAA, low-attenuation area; emphysema, defined as LAA%>10%; MLA E or I, mean lung attenuation value during expiration or inspiration. MLA I-E, difference between inspiratory and expiratory mean lung attenuation value. $\%CSA_{<5}$, percentage of total lung area taken up by the cross-sectional area of pulmonary vessels less than 5 mm^2; $\%CSA_{5–10}$, percentage of total lung area taken up by the cross-sectional area of pulmonary vessels between 5 and 10 mm^2; $CSN_{<5}$, number of vessels less than 5 mm^2 normalized by total lung area; CSN_{5-10}, number of vessels between 5 and 10 mm^2 normalized by total lung area; NR: not relevant. P values were calculated with the use of a two-sided independent t-test for variables with a parametric distribution, Fisher's exact test for comparison of proportions, and the Mann–Whitney U test for comparison of nonparametric variables.

Table 2: Association of high tissue fibrocyte density with COPD

Type of tissue	n	AUC ± SD	P value	Cut-off value	Sensitivity [IC]	Specificity [IC]
Distal	32	0.76 ± 0.09	0.04	72	0.83 [0.70-0.96]	0.70 [0.54-0.86]
Proximal	35	0.72 ± 0.09	0.02	32	0.79 [0.65-0.92]	0.67 [0.51-0.82]

Data are the absolute number with [95% confidence interval], and plus–minus values are the means ± SD. AUC, area under the ROC curve; ROC, receiver operating characteristic; SD, standard deviation. P values, sensitivity and specificity were evaluated for the ROC curve analysis.

Figures

Fig 1

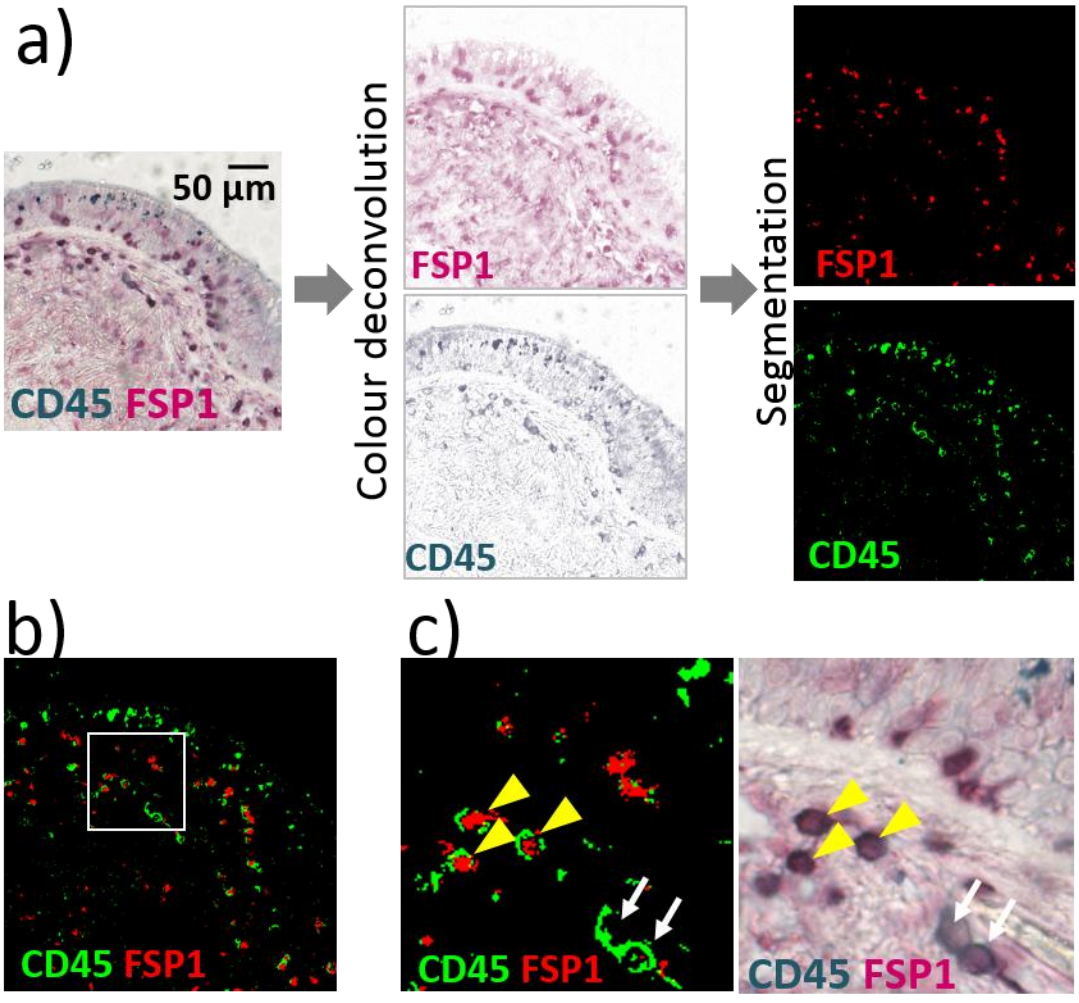

Fig 2

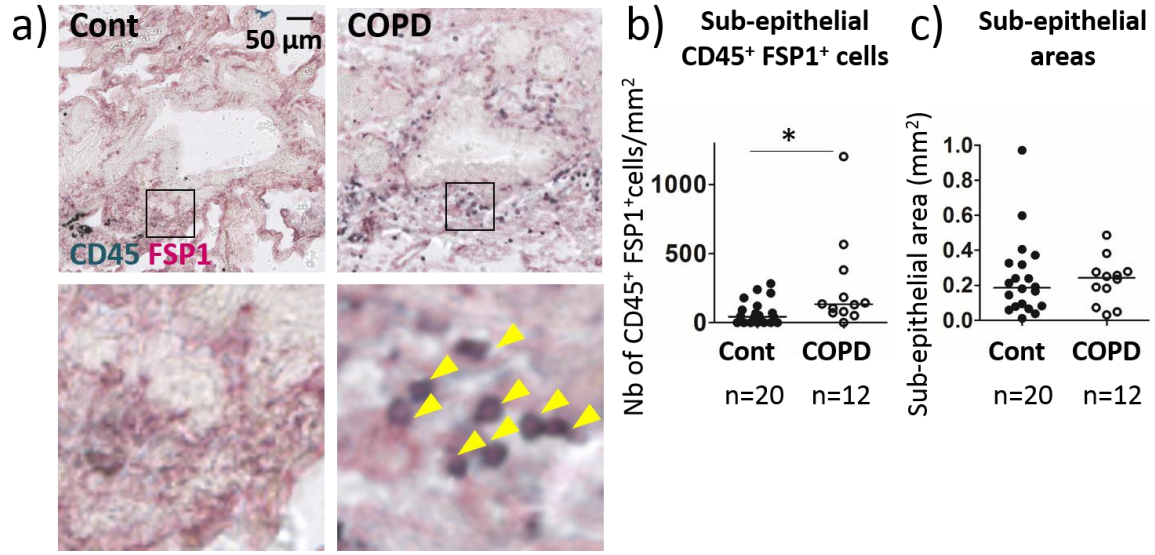
a)
Cont
50 µm
COPD
CD45 FSP1
b)
Sub-epithelial
CD45⁺ FSP1⁺ cells
Nb of CD45⁺ FSP1⁺cells/mm²
1000
500
0
*
Cont
COPD
n=20
n=12
c)
Sub-epithelial
areas
Sub-epithelial area (mm²)
1.0
0.8
0.6
0.4
0.2
0.0
Cont
COPD
n=20
n=12

Fig 3

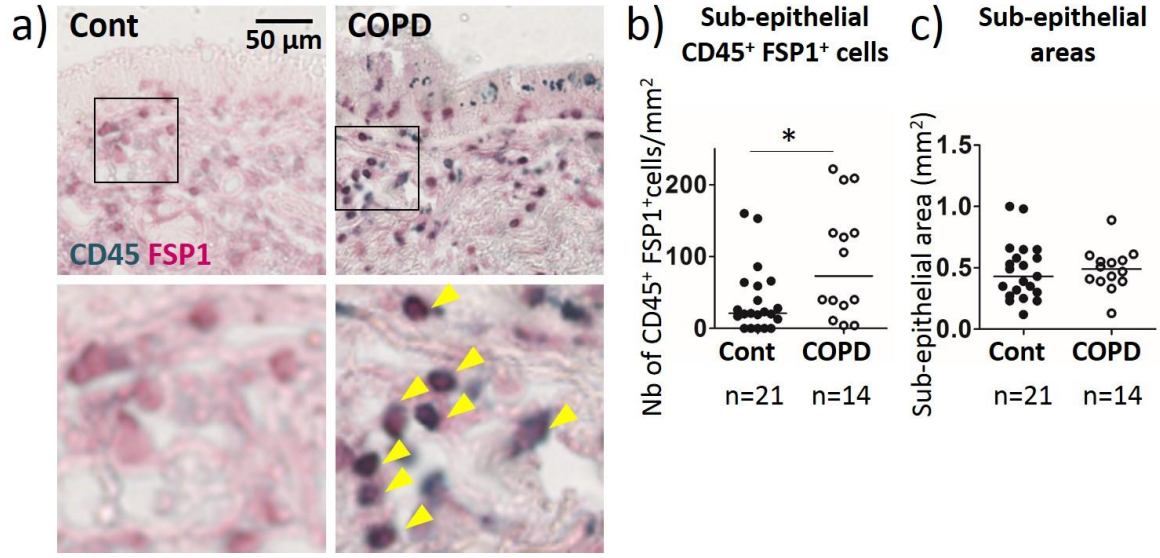
a)
Cont
50 µm
COPD
CD45 FSP1
b)
Sub-epithelial
CD45⁺ FSP1⁺ cells
Nb of CD45⁺ FSP1⁺cells/mm²
200
100
0
*
Cont
COPD
n=21
n=14
c)
Sub-epithelial
areas
Sub-epithelial area (mm²)
1.5
1.0
0.5
0.0
Cont
COPD
n=21
n=14

Fig 4

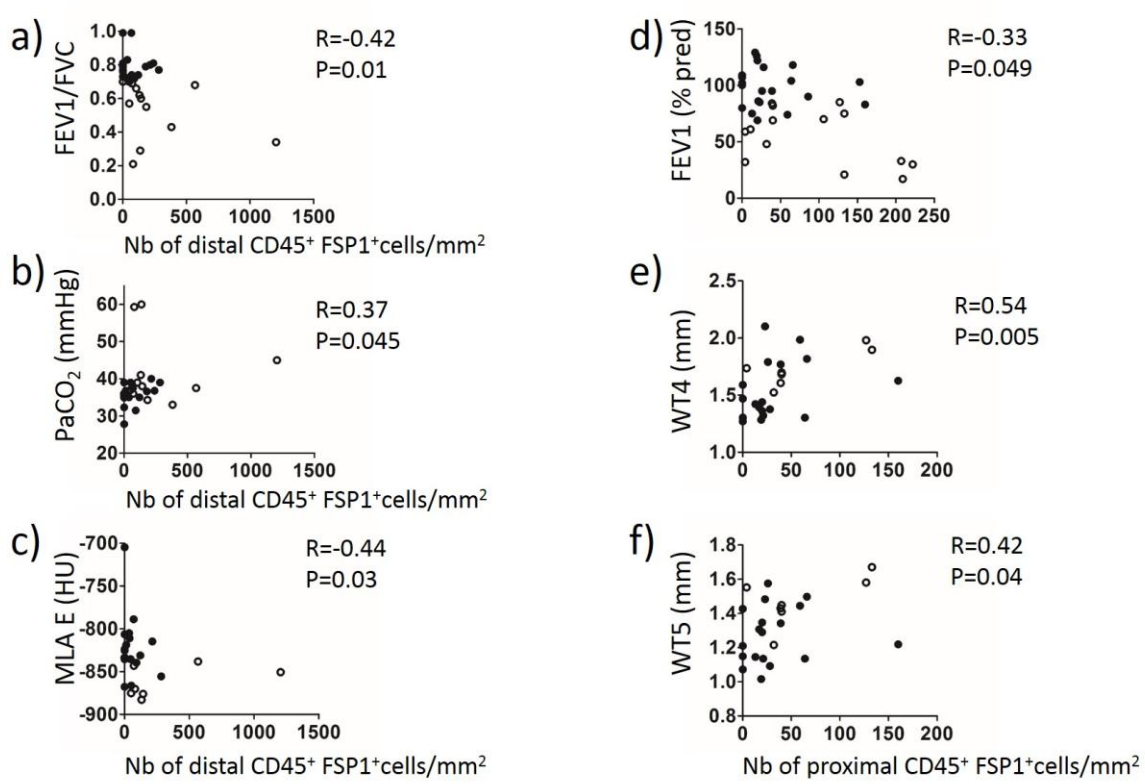
a)
FEV1/FVC
R=-0.42
P=0.01
Nb of distal CD45+ FSP1+cells/mm2
b)
PaCO2 (mmHg)
R=0.37
P=0.045
Nb of distal CD45+ FSP1+cells/mm2
c)
MLA E (HU)
R=-0.44
P=0.03
Nb of distal CD45+ FSP1+cells/mm2
d)
FEV1 (% pred)
R=-0.33
P=0.049
e)
WT4 (mm)
R=0.54
P=0.005
f)
WT5 (mm)
R=0.42
P=0.04
Nb of proximal CD45+ FSP1+cells/mm2

Fig 5

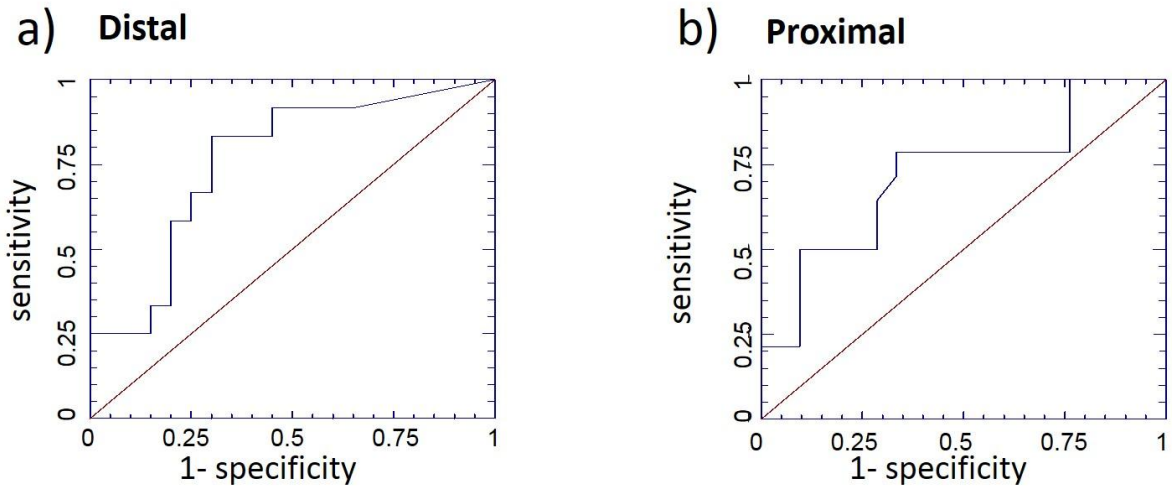
a) Distal
sensitivity
0
0.25
0.5
0.75
1
1- specificity
b) Proximal
sensitivity
0
0.25
0.5
0.75
1
1- specificity

Fibrocyte accumulation in the airway walls of COPD patients

Isabelle Dupin, Matthieu Thumerel, Elise Maurat, Florence Coste, Edmée Eyraud, Hugues Begueret, Thomas Trian, Michel Montaudon, Roger Marthan, Pierre-Olivier Girodet, Patrick Berger

Online Data Supplement

Supplemental Material and Methods

Study Populations

Subjects more than 40 years of age were eligible for enrolment if they required thoracic lobectomy surgery for cancer (pN0), lung transplantation or lung volume reduction (see Table E1 for individual indications). The size of the study was estimated from data obtained in patients with refractory asthma compared with non asthmatic subjects [1]. The expected difference between the two groups of interest (control subjects and COPD patients) is 4.5 fibrocytes / mm² with a standard deviation of 4.7. A total of 15 subjects per group is required for 80% power with an alpha risk of 0.05. All the study subjects were in stable status, as required for thoracic surgery. Only 5 patients experienced 1 or 2 exacerbations during the year before the study (patients n°24, 21, 49, 50, 51, see Table E1) whereas no exacerbation occurred during the last 2 months prior to surgery. A total of 17 COPD patients, with a clinical diagnosis of COPD according to the GOLD guidelines [2] and 25 non-COPD subjects ("control subjects") with normal lung function testing *(i.e.*, FEV_1/ FVC > 0.70) and no chronic symptoms (cough or expectoration) were recruited from the University Hospital of

Bordeaux. Main exclusion criteria for both COPD patients and control subjects were history of asthma, lung fibrosis, idiopathic pulmonary hypertension and chronic viral infections (hepatitis, HIV). The main withdrawal criterion for subjects included for lobectomy due to cancer was a staging different from pN0 confirmed after surgery.

To study fibrocyte survival *in vitro*, blood samples were obtained from a separate cohort of COPD patients. These patients were recruited from the COBRA cohort ("Cohorte Obstruction Bronchique et Asthme"; Bronchial Obstruction and Asthma Cohort; sponsored by the French National Institute of Health and Medical Research, INSERM), as outpatients in the Clinical Investigation Centre of the University Hospital of Bordeaux (Tables E4 and E6).

To assess the role of epithelium on fibrocyte survival *in vitro*, macroscopically normal, lung resection material was ethically obtained by lobectomy from a separate group of patients categorized into COPD and control groups as per GOLD criteria (Table E5).

All subjects provided written informed consent to participate to the study. All clinical data were collected in the Clinical Investigation Center (CIC1401) from the University Hospital of Bordeaux. The study protocol was approved by the research ethics committee ("CPP") and the French National Agency for Medicines and Health Products Safety ("ANSM").

Study design

The study protocol was approved by the local research ethics committee on May 30, 2012 and the French National Agency for Medicines and Health Products Safety on May 22, 2012. All clinical investigations have been conducted according to the principles expressed in the Declaration of Helsinki. All subjects provided written informed consent. The clinical trial was conducted from April 2013 (1^{st} patient, 1^{st} visit) to May 2016 (last patient, last visit). As already indicated, all patients undergoing surgery were thus recruited from the Department of

Thoracic Surgery of the University Hospital. The study was sponsored and funded by the University Hospital of Bordeaux (*i.e*. "CHU de Bordeaux"). All authors were academic and made the decision to submit the manuscript for publication and vouch for the accuracy and integrity of the contents. The study was registered at ClinicalTrials.gov under the N° NCT01692444 (*i.e.*, "Fibrochir" study).

The study design is summarized in Fig E1. The pre-inclusion visit (V1) before surgery, consisted of patient information and signature of the inform consent followed by a clinical evaluation (*i.e*., pulmonary auscultation, assessment of the WHO score, history of previous 12 months, smoking status, current treatment…). A full-body CT-scan with injection, was performed as part of the classical disease management but was preceded by two complementary thoracic acquisitions at expiration and inspiration without injection within the framework of the study. The patients also underwent echocardiography and lung function testing using body plethysmography, lung transfer capacity (TLCO) and arterial gas. The inclusion visit (V2), on the day of surgery, consisted of a clinical evaluation (*i.e*., control assessment test (CAT), St Georges Quality of Life Questionnaire (SGQLQ) and six-minute walk test) and venous blood sample (50 ml) for fibrocytes analysis. After thoracic surgery (lobectomy or pneumonectomy), a pulmonary sample from a grossly normal part of the surgical specimen is included in paraffin for subsequent analysis of the bronchial fibrocytes. Due to low quality of some tissue sections, fibrocyte density quantification was impossible in 10 distal specimens and 7 proximal specimens (Fig E1), which were excluded from peribronchial fibrocyte analysis. During hospital stay, clinical data was collected such as pTNM status for cancer patients. A visit one month ± 15 days after surgery (V3) consisted of spirometric evaluation. The final visit one year ± 15 days after surgery (V4) consisted of clinical (CAT, SGQLQ and six-minute walk test) and functional (plethysmography, TLCO, arterial gas) evaluations. COPD patients and control subjects performed the whole series of

"Fibrochir" visits, with the exception of 2 COPD patients who provided written informed consent for the use of biological samples and clinical data for research and underwent only two visits (corresponding to V1 and V2) including the surgical pulmonary sample for peribronchial fibrocyte analysis.

Bronchial fibrocyte identification

A sub-segmental bronchus sample (for proximal tissue) and as fragments of distal parenchyma were obtained from lung resection material, at distance from the tumor in case of cancer. Additional proximal samples from the upper lobes and lower lobes were obtained from 4 transplanted patients (patient numbers 48, 49, 51, and 52, see Table E1) to compare fibrocyte density in different lobes. The samples were embedded in paraffin and 2.5 µm thick sections were cut, as described previously [3]. Sections were deparaffinized through three changes of xylene and through graded alcohols to water. Heat induced antigen retrieval was performed using citrate buffer, pH 6 (Fisher Scientific, Illkirch, France) in a Pre-Treatment Module (Agilent, Les Ulis, France). Endogenous peroxidase and alkaline phosphatases (AP) were blocked for 10 min using Dual Enzyme Block (Diagomics, Blagnac, France). Nonspecific binding was minimized by incubating the sections with 4% Goat Serum (Agilent) for 30 min. The sections were stained with both rabbit anti-FSP1 polyclonal antibody (Agilent) and mouse anti-CD45 monoclonal antibody (BD Biosciences, San Jose, CA), or mouse anti-CD3 monoclonal antibody (Agilent), mouse anti-CD19 monoclonal (Agilent), mouse anti-CD34 monoclonal antibody (Agilent) or appropriate isotype controls, rabbit IgG (Fisher Scientific) and mouse IgG1 (R&D Systems, Lille, France) at the same concentration. For CD45-FSP1 double staining, the sections were re-incubated with HRP-Polymer anti-Mouse and AP Polymer anti-Rabbit antibodies (Diagomics). Sections were developed with

the chromogenic substrates, GBI-Permanent Red and Emerald. For CD3-FSP1, CD19-FSP1 and CD34-FSP1 double staining, the sections were re-incubated with HRP anti-Mouse (Agilent) and with Alexa488–conjugated anti-Rabbit (Fisher Scientific) antibodies. Immunoreactivity was detected by using the DAB System (Agilent) for CD3, CD19 or CD34 staining and by fluorescence for FSP1 staining.

The sections were imaged using a slide scanner Nanozoomer 2.0HT with fluorescence imaging module (Hamamatsu Photonics, Massy, France) using objective UPS APO 20X NA 0.75 combined to an additional lens 1.75X, leading to a final magnification of 35X. Virtual slides were acquired with a TDI-3CCD camera. Fluorescent acquisitions were done with a mercury lamp (LX2000 200W - Hamamatsu Photonics) and the set of filters adapted for DAPI and Alexa 488. Bright field and fluorescence images where acquired with the NDP-scan software (Hamamatsu) and processed with ImageJ. Quantification of FSP1 and CD45 double-positive cells was performed as described in Fig 1. A color deconvolution plugin was used on bright field image to separate channels corresponding to GBI-Permanent Red and Emerald double staining, and a binary threshold was then applied to these images (Fig 1a). Tissue fibrocytes were defined as cells dual positive for cytoplasmic FSP1 and plasma membrane CD45 double staining on the merged threshold image (Fig 1b-c). The lamina propria contour was manually determined on bright field image and the area was calculated. For distal bronchi, the lumen area was also determined and only bronchi less than 2 mm in diameter were analyzed as described by J.C. Hogg *et al* [4]. The density of $FSP1^+$ $CD45^+$ cells was defined by the ratio between the numbers of double-positive cells in the lamina propria divided by the lamina propria area. Quantification of double-positive FSP1 and CD3, FSP1 and CD19 or FSP1 and CD34 cells was performed as described above with some modifications: a color deconvolution plugin was used on bright field image to select the channel corresponding to DAB signal (for CD3, CD19 or CD34 staining), and a binary

threshold was then applied to this image and fluorescence image corresponding to FSP1 staining. Tissue area and cell measurements were all performed in a blinded fashion for patient characteristics.

Quantitative computed tomography

CT scans were performed on a Somatom Sensation Definition 64 (Siemens, Erlangen, Germany) at full inspiration and expiration, as described previously [5-8]. Briefly, quantitative analysis was performed by using dedicated and validated software: Automatic quantification of bronchial wall area (WA), lumen area (LA), WA/LA (WA%) and wall thickness (WT) was obtained on orthogonal bronchial cross sections by using the Laplacian-of-Gaussian algorithm and homemade software [9, 10]; Automatic quantification of both emphysema and air trapping was assessed using Myrian software (Intrasense, Montpellier, France) and both low attenuation area per cent (LAA%) [5, 6] and mean lung attenuation (MLA) during expiration [7, 8]; Quantification of pulmonary vessels was obtained from CT images, as previously described [5]. Briefly, CT set of images reconstructed with sharp algorithm (B70f) were analyzed by using the ImageJ software version 1.40g (a public domain Java image program available at http://rsb.info.nih.gov/ij/). The small pulmonary vessels measurements were made automatically as described elsewhere [5, 11-13]. The cross section area (CSA) and cross section number (CSN) of small pulmonary vessels were quantified separately at the subsegmental and at the sub-subsegmental levels [5, 13]. The subsegmental and sub-subsegmental levels are defined by a vessel area between 5 and 10 mm^2 and less than 5 mm^2, respectively. Finally, quantifications were obtained after normalization by the corresponding lung section area at each CT slice: the cross sectional area of small pulmonary vessel less than 5 mm^2 ($\%CSA_{<5}$). Four measurements were obtained after normalization by

the corresponding lung section area at each CT slice: the cross sectional area of small pulmonary vessel between 5 to 10 mm^2 ($\%CSA_{5-10}$), and less than 5 mm^2 ($\%CSA_{<5}$), the mean number of cross-sectioned vessels CSN_{5-10} and $CSN_{<5}$. Emphysematous patients were defined as patients with a LAA% > 10% [14].

Circulating fibrocyte identification

Non-adherent non-T (NANT) cells were purified from peripheral blood mononuclear cells (PBMCs) separated from the whole blood, and circulating fibrocytes were identified as double positive cells for the surface marker CD45 and the intracellular marker collagen I by flow cytometry, as described previously [15]. Briefly, PBMCs were first separated from the whole blood by Ficoll-Hypaque (Dutscher, Brumath, France) density gradient centrifugation. The non-adherent mononuclear cell fraction was taken and washed in cold PBS containing 0.5% bovine serum albumin (BSA, Sigma-Aldrich) and 2 mM Ethylene Diamine Tetra-acetic Acid (EDTA, Invitrogen). T-cells were further depleted with anti-CD3 monoclonal antibody (Miltenyi Biotech, Paris, France). Cells were fixed overnight with Cytofix/Cytoperm (eBioscience, Paris, France), washed in permeabilization buffer (eBioscience) and incubated either with mouse anti-human collagen I antibody (Millipore, St-Quentin-en-Yvelines, France) or with matched IgG1 isotype control (Santa Cruz Biotechnology, Heidelberg, Germany), followed by fluorescein isothiocyanate (FITC)–conjugated anti-mouse antibodies (Beckman Coulter, Villepinte, France). Next, the cell pellet was incubated either with allophycocyanin (APC)-conjugated anti-CD45 antibodies (BD Biosciences, San Jose, CA) or with matched APC-conjugated IgG1 isotype control (BD Biosciences). The cell suspension was analyzed with a BD FACSCanto II flow cytometer (BD Biosciences). Offline analysis was performed with FACSDiva (BD Biosciences) and FlowJo (Tree Star, Ashland, OR) software. The negative threshold for CD45 was set using a matched APC-conjugated IgG1

isotype control, and all subsequent samples were gated for the CD45 positive region. Cells gated for CD45 were analyzed for collagen I expression, with negative control thresholds set using FITC-stained cells. Specific staining for collagen I was determined as an increase in positive events over this threshold. Fibrocytes numbers were expressed as both a percentage of total PBMC counts and as absolute number of cells.

Bronchial epithelial supernatants

Human bronchial epithelial cells (BECs) were derived from bronchial specimens as described previously [16]. Bronchial epithelial tissue was cultured in bronchial epithelial growth medium (Stemcell, Grenoble, France) in a flask (0.75 cm^2). After confluence, basal BEC were plated (2.10^5 cells per well) on uncoated nucleopore membranes (24-mm diameter, 0.4-µm pore size, Transwell Clear; Costar, Cambridge, Mass) in ALI medium (Stemcell) applied at the basal side only to establish the air-liquid interface. Cells were maintained in culture for 21 days to obtain a differentiated cell population with a mucociliary phenotype. Basal epithelial supernatant was collected every 2-3 days and used for further experiments.

Fibrocyte differentiation and survival

A total of 2.10^6 NANT cells resuspended in 0.2 ml DMEM (Fisher Scientific), containing 4.5 g/l glucose and glutaMAX, supplemented with 20% foetal calf serum (Biowest, Riverside, USA), penicillin/streptomycin and MEM non-essential amino acid solution (Sigma-Aldrich), was added to each well of a 6 well plate. After one week in culture, fibrocyte differentiation was induced by changing the medium for a serum-free medium (Fig E2), or for a serum-free medium containing 50% of basal epithelium supernatant (Fig E14). Mediums were changed every 2-3 days. After 2 weeks in culture, the cells were detached by accutase treatment (Fisher Scientific), fixed overnight with Cytofix/Cytoperm and washed in permeabilization buffer (for collagen-CD45-FSP1 stainings) or fixed with 4% paraformaldehyde solution and

washed in PBS containing 0.5% BSA, 2 mM EDTA, 0.5% Tween (Sigma-Aldrich) (for the other stainings). Cells were incubated overnight with rabbit anti-FSP1 polyclonal antibody (Agilent) or with matched IgG isotype control (Fisher Scientific), and either with FITC–conjugated mouse anti-human collagen I antibody (Millipore) or with matched FITC-conjugated IgG1 isotype control (Millipore). Next, the cell pellet was incubated with Phycoerythrin (PE)–conjugated anti-rabbit antibody (Santa Cruz Biotechnology, Heidelberg, Germany) and with FITC-conjugated mouse IgGκ binding protein (Santa Cruz Biotechnology). Cells were then incubated with APC-conjugated anti-CD45 antibody or with matched APC-conjugated IgG1 isotype control, and either with FITC–conjugated mouse anti-human vimentin antibody (Santa Cruz), FITC–conjugated mouse anti-human fibronectin antibody (Santa Cruz) or with matched FITC-conjugated IgG1 isotype control (Santa Cruz), or FITC–conjugated mouse anti-human α-smooth muscle actin (α-SMA) antibody (Sigma-Aldrich) or with matched FITC-conjugated IgG2A isotype control (Sigma-Aldrich). The cell suspension was analyzed with a BD FACSCanto II flow cytometer. Cells gated for CD45 and FSP1 were analyzed for collagen-1, fibronectin, vimentin and α-SMA expression, with negative control thresholds set using isotype-stained cells. Specific staining for collagen I, fibronectin, vimentin and α-SMA was determined as an increase in positive events over this threshold.

Alternatively, after 2 weeks in culture, cells were fixed with 4% paraformaldehyde solution and stained for collagen I, fibronectin, vimentin, α-SMA, FSP1 and with DAPI (Fisher Scientific). Fixed cells were imaged on a microscope (Eclipse 80i, Nikon) using a HCX plan Fluor 40X/0.75 dry objective (Nikon).

Propidium iodide (Fisher Scientific) was used for the detection of dying cells. After 2 weeks in culture, cells detached by accutase treatment were used to prepare single cell suspension at

1.10^6 cells/ml. After addition of propidium iodide, the dying cells (PI^+ cells) were detected by flow cytometry (BD Biosciences).

Statistical analysis

Primary outcome was the density of bronchial fibrocytes in both distal and proximal airways. Secondary outcomes were lung function parameters, CT parameters and the percentage of blood fibrocytes in PBMCs. The statistical analysis was performed with Prism 6 software (GraphPad, La Jolla, CA) and NCSS software (NCSS 2001, Kaysville, UT, USA). Values are presented as the medians with individual plots or means ± SD. Statistical significance, defined as $P < 0.05$, was analysed by Fisher's exact test for the comparison of proportions, by two-sided independent t-test for variables with a parametric distribution, and by Wilcoxon test, Mann–Whitney U test and Spearman's correlation coefficient for variables with a non-parametric distribution. Concerning correlation analyses, no mathematical correction was made for multiple comparisons, as recommended [17]. A receiver operating characteristic (ROC) curves were built with NCSS software (NCSS 2001, Kaysville, UT, USA) and ROC analysis were performed to determine areas under the curve (AUC) and cut-off values for the best fibrocytes density in distal and proximal tissue specimens to predict COPD. Those 2 cut-off values were then used to evaluate the association between COPD and a high density of tissue fibrocytes using a univariate logistic regression analysis. To test potential sex differences, we performed subgroup analysis in control and COPD patients by matching them for sex (sex ratio: 0.5) and age.

References

1. Saunders R, Siddiqui S, Kaur D, Doe C, Sutcliffe A, Hollins F, Bradding P, Wardlaw A, Brightling CE. Fibrocyte localization to the airway smooth muscle is a feature of asthma. *J Allergy Clin Immunol* 2009: 123(2): 376-384.
2. GOLD 1998. Global Initiative for Chronic Obstructive Lung Disease. Global Strategy for the Diagnosis, Management and Prevention of Chronic Obstructive Pulmonary Disease. NIH Publication (updated 2019). Accessed January 1, 2019, at http://www.goldcopd.org.
3. Begueret H, Berger P, Vernejoux JM, Dubuisson L, Marthan R, Tunon-de-Lara JM. Inflammation of bronchial smooth muscle in allergic asthma. *Thorax* 2007: 62(1): 8-15.
4. Hogg JC, Chu F, Utokaparch S, Woods R, Elliott WM, Buzatu L, Cherniack RM, Rogers RM, Sciurba FC, Coxson HO, Pare PD. The nature of small-airway obstruction in chronic obstructive pulmonary disease. *N Engl J Med* 2004: 350(26): 2645-2653.
5. Coste F, Dournes G, Dromer C, Blanchard E, Freund-Michel V, Girodet PO, Montaudon M, Baldacci F, Picard F, Marthan R, Berger P, Laurent F. CT evaluation of small pulmonary vessels area in patients with COPD with severe pulmonary hypertension. *Thorax* 2016: 71(9): 830-837.
6. Dournes G, Laurent F, Coste F, Dromer C, Blanchard E, Picard F, Baldacci F, Montaudon M, Girodet PO, Marthan R, Berger P. Computed tomographic measurement of airway remodeling and emphysema in advanced chronic obstructive pulmonary disease. Correlation with pulmonary hypertension. *Am J Respir Crit Care Med* 2015: 191(1): 63-70.
7. Girodet PO, Dournes G, Thumerel M, Begueret H, Dos Santos P, Ozier A, Dupin I, Trian T, Montaudon M, Laurent F, Marthan R, Berger P. Calcium Channel Blocker Reduces Airway Remodeling in Severe Asthma. A Proof-of-Concept Study. *Am J Respir Crit Care Med* 2015: 191(8): 876-883.
8. Berger P, Laurent F, Begueret H, Perot V, Rouiller R, Raherison C, Molimard M, Marthan R, Tunon-de-Lara JM. Structure and function of small airways in smokers: relationship between air trapping at CT and airway inflammation. *Radiology* 2003: 228(1): 85-94.
9. Berger P, Perot V, Desbarats P, Tunon-de-Lara JM, Marthan R, Laurent F. Airway wall thickness in cigarette smokers: quantitative thin-section CT assessment. *Radiology* 2005: 235(3): 1055-1064.
10. Montaudon M, Berger P, de Dietrich G, Braquelaire A, Marthan R, Tunon-de-Lara JM, Laurent F. Assessment of airways with three-dimensional quantitative thin-section CT: in vitro and in vivo validation. *Radiology* 2007: 242(2): 563-572.
11. Uejima I, Matsuoka S, Yamashiro T, Yagihashi K, Kurihara Y, Nakajima Y. Quantitative computed tomographic measurement of a cross-sectional area of a small pulmonary vessel in nonsmokers without airflow limitation. *Jpn J Radiol* 2011: 29(4): 251-255.
12. Matsuoka S, Washko GR, Dransfield MT, Yamashiro T, San Jose Estepar R, Diaz A, Silverman EK, Patz S, Hatabu H. Quantitative CT measurement of cross-sectional area of small pulmonary vessel in COPD: correlations with emphysema and airflow limitation. *Acad Radiol* 2010: 17(1): 93-99.
13. Matsuoka S, Washko GR, Yamashiro T, Estepar RS, Diaz A, Silverman EK, Hoffman E, Fessler HE, Criner GJ, Marchetti N, Scharf SM, Martinez FJ, Reilly JJ, Hatabu H, National Emphysema Treatment Trial Research G. Pulmonary hypertension and computed tomography measurement of small pulmonary vessels in severe emphysema. *Am J Respir Crit Care Med* 2010: 181(3): 218-225.
14. Johannessen A, Skorge TD, Bottai M, Grydeland TB, Nilsen RM, Coxson H, Dirksen A, Omenaas E, Gulsvik A, Bakke P. Mortality by level of emphysema and airway wall thickness. *Am J Respir Crit Care Med* 2013: 187(6): 602-608.
15. Dupin I, Allard B, Ozier A, Maurat E, Ousova O, Delbrel E, Trian T, Bui HN, Dromer C, Guisset O, Blanchard E, Hilbert G, Vargas F, Thumerel M, Marthan R, Girodet PO, Berger P. Blood fibrocytes are recruited during acute exacerbations of chronic obstructive pulmonary disease through a CXCR4-dependent pathway. *J Allergy Clin Immunol* 2016: 137(4): 1036-1042 e1037.
16. Trian T, Allard B, Dupin I, Carvalho G, Ousova O, Maurat E, Bataille J, Thumerel M, Begueret H, Girodet PO, Marthan R, Berger P. House dust mites induce proliferation of severe

asthmatic smooth muscle cells via an epithelium-dependent pathway. *Am J Respir Crit Care Med* 2015: 191(5): 538-546.
17. Rothman KJ. No adjustments are needed for multiple comparisons. *Epidemiology* 1990: 1(1): 43-46.

Supplemental tables

Table E1. Indications for thoracic surgery

Patient number	Classification (cont vs COPD)	Tumor stage*/ Lung transplantation (LT)	Tumor histology
1	Cont	pT1	lepidic adenocarcinoma
2	Cont	pT2	papillary and lepidic adenocarcinoma
3	Cont	pT2	mucinous adenocarcinoma
4	Cont	pT2	mucinous adenocarcinoma
8	Cont	pT2	adenocarcinoma
9	Cont	pT1	mucinous adenocarcinoma
11	Cont	pT3	typical carcinoid
12	Cont	pT2	lepidic adenocarcinoma
13	Cont	pT1	squamous cell carcinoma
15	Cont	pT0	Abrikossoff tumor
16	Cont	pT1	acinar adenocarcinoma
24	Cont	pT2	atypical carcinoid
27	Cont	pT2	acinar adenocarcinoma
28	Cont	pT1	acinar adenocarcinoma
29	Cont	pT1	lepidic adenocarcinoma
31	Cont	pT2	acinar adenocarcinoma
33	Cont	pT1	papillary adenocarcinoma
34	Cont	pT1	adenocarcinoma
37	Cont	pT2	acinar adenocarcinoma
39	Cont	pT1	acinar adenocarcinoma
41	Cont	pT3	squamous cell carcinoma
43	Cont	pT1	adenocarcinoma
44	Cont	pT1	adenocarcinoma
46	Cont	pT2	acinar adenocarcinoma
47	Cont	pT1	acinar adenocarcinoma
7	COPD	pT1	squamous cell carcinoma
10	COPD	pT1	squamous cell carcinoma
17	COPD	pT3	acinar adenocarcinoma
18	COPD	pT2	acinar adenocarcinoma
21	COPD	pT1	adenocarcinoma
22	COPD	pT0	benign nodule
23	COPD	pT1	small cell carcinoma
26	COPD	pT1	small cell carcinoma
32	COPD	pT0	adenocarcinoma
36	COPD	pT1	papillary adenocarcinoma
42	COPD	pT1	acinar adenocarcinoma
45	COPD	pT1	acinar adenocarcinoma
48	COPD	LT	NR
49	COPD	LT	NR
50	COPD	LT	NR
51	COPD	LT	NR
52	COPD	LT	NR

* All the tumors are N0M0.

Cont: Control subject; LT: Lung transplantation; NR: not relevant.

Table E2. Association between distributions of distal tissue fibrocytes and COPD clinical characteristics

	Distal $CD45^+$ $FSP1^+$ cells density		
	Spearman r	**95% confidence interval**	**P value**
Age (yrs.)	0.06	[-0.31-0.41]	0.76
Body-mass index (kg/m^2)	0.09	[-0.28-0.43]	0.63
Pack years (no.)	0.21	[-0.17-0.53]	0.26
LFT			
FEV_1 (% pred.)	-0.28	[-0.58-0.08]	0.12
FEV_1/FVC ratio (%)	-0.42	[-0.68-0.07]	**0.02**
FVC (% pred.)	-0.31	[-0.60-0.06]	0.09
RV (% pred.)	0.30	[-0.06-0.59]	0.10
TLCO (% pred.)	-0.20	[-0.53-0.20]	0.31
Six-minute walk test distance (m)	0.14	[-0.26-0.49]	0.49
Arterial blood gases	-0.27	[-0.58-0.11]	0.15
PaO_2 (mm Hg)	0.37	[-0.002-0.65]	**0.04**
$PaCO_2$ (mm Hg)			
CT parameters			
Bronchi:	0.12	[-0.31-0.50]	0.56
WA4%	0.08	[-0.33-0.47]	0.68
WT4 (mm)	0.29	[-0.13-0.62]	0.16
WA5%	0.17	[-0.25-0.54]	0.41
WT5 (mm)			
Emphysema:	0.36	[-0.01-0.64]	0.056
LAA (%)			
Air trapping:	-0.44	[-0.72-0.03]	**0.03**
MLA E (HU)	-0.20	[-0.54-0.20]	0.31
MLA I (HU)	0.08	[-0.35-0.48]	0.72
MLA I-E (HU)			
Pulmonary Vessels	-0.21	[-0.54-0.16]	0.26
$\%CSA_{<5}$	-0.15	[-0.49-0.24]	0.44
$\%CSA_{5-10}$	-0.18	[-0.52-0.19]	0.33
$CSN_{<5}$	-0.16	[-0.38-0.36]	0.41
CSN_{5-10}			

FEV_1, forced expiratory volume in 1 second; FVC, forced vital capacity; LFT, lung function test; RV, residual volume; TLCO, Transfer Lung capacity of Carbon monoxide, PaO_2, partial arterial oxygen pressure, $PaCO_2$, partial arterial carbon dioxide pressure; WA, mean wall area; LA, mean lumen area, WA%, mean wall area percentage; WT, wall thickness; LAA, low-attenuation area; MLA E or I, mean lung attenuation value during expiration or inspiration. MLA I-E, difference between inspiratory and expiratory mean lung attenuation value. $\%CSA_{<5}$, percentage of total lung area taken up by the cross-sectional area of pulmonary vessels less than 5 mm^2; $\%CSA_{5–10}$, percentage of total lung area taken up by the cross-sectional area of pulmonary vessels between 5 and 10 mm^2; $CSN_{<5}$, number of vessels less than 5 mm^2 normalized by total lung area; CSN_{5-10}, number of vessels between 5 and 10 mm^2 normalized by total lung area; NR: not relevant. The correlation coefficient (r), 95% confidence interval and significance level (P value), were obtained by using nonparametric Spearman analysis.

Table E3. Association between distributions of proximal tissue fibrocytes and COPD clinical characteristics

	Proximal $CD45^+$ $FSP1^+$ cells density		
	Spearman r	**95% confidence interval**	**P value**
Age (yrs.)	-0.09	[-0.42-0.26]	0.60
Body-mass index (kg/m^2)	0.32	[-0.03-0.60]	0.06
Pack years (no.)	0.02	[-0.34-0.38]	0.91
LFT			
FEV_1 (% pred.)	-0.33	[-0.61-0.009]	**0.049**
FEV_1/FVC ratio (%)	-0.28	[-0.57-0.07]	0.10
FVC (% pred.)	-0.34	[-0.61-0.005]	**0.04**
RV (% pred)	0.43	[0.10-0.67]	**0.01**
TLCO (% pred.)	-0.04	[-0.40-0.32]	0.80
Six-minute walk test distance (m)	-0.14	[-0.48-0.24]	0.46
Arterial blood gases			
PaO_2 (mm Hg)	-0.26	[-0.55-0.09]	0.14
$PaCO_2$ (mm Hg)	0.20	[-0.16-0.50]	0.26
CT parameters			
Bronchi:			
WA4%	0.50	[0.11-0.75]	**0.02**
WT4 (mm)	0.54	[0.18-0.78]	**0.005**
WA5%	0.34	[-0.08-0.65]	0.10
WT5 (mm)	0.42	[0.008-0.70]	**0.04**
Emphysema:			
LAA (%)	0.18	[-0.20-0.51]	0.34
Air trapping:			
MLA E (HU)	0.07	[-0.35-0.46]	0.76
MLA I (HU)	0.08	[-0.31-0.44]	0.68
MLA I-E (HU)	0.28	[-0.14-0.62]	0.17
Pulmonary Vessels			
$\%CSA_{<5}$	-0.07	[-0.42-0.31]	0.73
$\%CSA_{5-10}$	-0.06	[-0.43-0.29]	0.77
$CSN_{<5}$	-0.03	[-0.40-0.33]	0.88
CSN_{5-10}	-0.07	[-0.36-0.36]	0.70

LFT, lung function test; FEV_1, forced expiratory volume in 1 second; FVC, forced vital capacity; RV, residual volume; TLCO, Transfer Lung capacity of Carbon monoxide, PaO_2, partial arterial oxygen pressure, $PaCO_2$, partial arterial carbon dioxide pressure; WA, mean wall area; LA, mean lumen area, WA%, mean wall area percentage; WT, wall thickness; LAA, low-attenuation area; MLA E or I, mean lung attenuation value during expiration or inspiration. MLA I-E, difference between inspiratory and expiratory mean lung attenuation value. $\%CSA_{<5}$, percentage of total lung area taken up by the cross-sectional area of pulmonary vessels less than 5 mm^2; $\%CSA_{5–10}$, percentage of total lung area taken up by the cross-sectional area of pulmonary vessels between 5 and 10 mm^2; $CSN_{<5}$, number of vessels less than 5 mm^2 normalized by total lung area; CSN_{5-10}, number of vessels between 5 and 10 mm^2 normalized by total lung area; NR: not relevant. The correlation coefficient (r), 95% confidence interval and significance level (P value), were obtained by using nonparametric Spearman analysis.

Table E4. Patient characteristics

	COPD
n	9
Age (yr)	67.1 ± 9.9
Sex (Men/Woman)	7/2
Body-mass index (kg/m^2)	25.4 ± 6.3
Current smoker (Y/N)	5/4
Former smoker (Y/N)	4/5
Pack years (no.)	50.3 ± 15.1
PFT	
FEV_1 (% pred.)	59.8 ± 19.3
FEV_1/FVC ratio (%)	54.9 ± 9.4
FVC (% pred.)	84.5 ± 18.1
Six-minute walk test distance (m)	493 ± 159
Arterial blood gases	
PaO_2 (mm Hg)	70.3 ± 11.8
$PaCO_2$ (mm Hg)	39.4 ± 5.1

Plus–minus values indicate means ± SD. PFT, pulmonary function test; FEV_1, forced expiratory volume in 1 second; FVC, forced vital capacity; PaO_2, partial arterial oxygen pressure, $PaCO_2$, partial arterial carbon dioxide pressure.

Table E5. Patient characteristics (for bronchial epithelial supernatants production)

	COPD	Control
n	2	2
Age (yr)	62.5 ± 12.0	70.5 ± 13.4
Sex (Men/Woman)	0/2	2/0
Body-mass index (kg/m^2)	31.5 ± 7.8	24.5 ± 0.7
Current smoker (Y/N)	0/1*	0/2
Former smoker (Y/N)	1/0*	0/2
Pack years (no.)	50.0 ± 70.7	0
PFT		
FEV_1 (% pred.)	62.5 ± 3.5	113.5 ± 62.9
FEV_1/FVC ratio (%)	61.0 ± 0	81.5 ± 0.1

Plus–minus values indicate means ± SD. PFT, pulmonary function test; FEV_1, forced expiratory volume in 1 second; FVC, forced vital capacity. * one of the two COPD patients has been professionally exposed to noxious particles.

Table E6. Patient characteristics

	COPD
n	6
Age (yr)	69.2 ± 8.0
Sex (Men/Woman)	2/4
Body-mass index (kg/m^2)	27.7 ± 5.6
Current smoker (Y/N)	4/2
Former smoker (Y/N)	2/4
Pack years (no.)	66.3 ± 24.7
PFT	
FEV_1 (% pred.)	67.1 ± 22.5
FEV_1/FVC ratio (%)	62.1 ± 6.4
FVC (% pred.)	86.2 ± 30.0
Six-minute walk test distance (m)	395 ± 187
Arterial blood gases	
PaO_2 (mm Hg)	71.1 ± 6.6
$PaCO_2$ (mm Hg)	37.1 ± 4.7

Plus–minus values indicate means ± SD. PFT, pulmonary function test; FEV_1, forced expiratory volume in 1 second; FVC, forced vital capacity; PaO_2, partial arterial oxygen pressure, $PaCO_2$, partial arterial carbon dioxide pressure.

Supplemental figures legends

Supplementary Fig E1. Study design.

Numbers of patients who were included and had fibrocyte density quantification in the proximal and distal airways.

Supplementary Fig E2. $CD45^+$ $FSP1^+$ cells purified from NANT cells express collagen I, fibronectin, vimentin and α-smooth muscle actin after 2 weeks of differentiation in culture.

a-c, Representative dot plots of flow cytometry for CD45, FSP1, collagen I, fibronectin, vimentin and α-smooth muscle actin (α-SMA) expression. a, Left panel: total Non-Adherent Non T (NANT) cell population selected on the scatter plot of FSC-A vs SSC-A. Middle and right panels: a gate ($CD45^+$ and $FSP1^+$) was drawn in FSP1-PE vs APC-CD45 dot plot to define the Q2 population (positive population for both CD45 and FSP1). b-c, a gate was drawn in each histogram to define the P3 population (positive population for CD45, FSP1 and collagen I/fibronectin/vimentin/α-SMA). b, isotype control for collagen I, fibronectin, vimentin and α-SMA. c, colI, fibronectin, vimentin and α-SMA stainings. APC: allophycocyanin; FITC: fluorescein isothiocyanate; PE: Phycoerythrin; FSC-A: forward scatter; SSC-A: side scatter. d, Representative images of immunocytochemistry for CD45, FSP1, collagen I, fibronectin, vimentin and α-SMA expression. The upper left and right panels show respectively CD45 (magenta) and FSP1 (cyan) stainings, and the lower panel shows a higher magnification of fibronectin, vimentin or α-SMA (all in green) stainings with DAPI (blue). Bar, 10 μm.

Supplementary Fig E3. Presence of fibrocytes in peribronchial area outside the smooth muscle layer.

Representative staining of CD45 (green) and FSP1 (red) in distal (left) and proximal (right) bronchial tissue specimens. The lower panels show higher magnification of the small area (black boxes) defined in the upper panels. The smooth muscle layer has been highlighted in orange. The yellow arrowheads indicate fibrocytes, defined as $CD45^+$ $FSP1^+$ cells.

Supplementary Fig E4. Relationship between the density of $CD45^+$ $FSP1^+$ cells in proximal airways and that in distal airways.

Densities measured in control subjects and COPD patients are represented respectively with black and open circles. The correlation coefficient (r) and significance level (P value) were obtained by using nonparametric Spearman analysis.

Supplementary Fig E5. Fibrocyte density in upper lobes in comparison with that in lower or middle lobes

a, b, Quantification of fibrocyte density (normalized by the sub-epithelial area) in one specimen/patient in distal (a) and proximal (b) tissue specimens. Fibrocyte densities measured in upper lobes (“Up”, pink squares) were compared to the densities measured in lower or middle lobes (“Low+Middle”, green squares). The medians are represented as horizontal lines. c, Comparison of fibrocyte density in transplanted patients (n=4) in upper lobes (“Up”, pink squares) and lower lobes (“Low”, green squares) in proximal tissue specimens.

Supplementary Fig E6. Increased fibrocyte density in distal and proximal airways of COPD patients, in comparison with control smokers

a, b, Quantification of fibrocyte density (normalized by the sub-epithelial area) in distal (a) and proximal (b) tissue specimens. The medians are represented as horizontal lines. *: $P<0.05$, Mann Whitney test.

Supplementary Fig E7. Fibrocyte density in distal and proximal airways and relationships between fibrocyte density, lung function parameters and CT parameters in sex and age matched patients

a, b, Quantification of fibrocyte density (normalized by the sub-epithelial area) in one specimen/patient in distal (a) and proximal (b) tissue specimens. COPD and control patients were matched for sex (sex ratio: 0.5) and age. Medians are represented as horizontal lines. *: $P<0.05$, Mann Whitney test. c, e, g, Relationships between FEV1/FVC (c), PaO_2 (e), MLA during expiration (g) and the density of $CD45^+$ $FSP1^+$ cells in distal airways measured in control subjects (black circles) and COPD patients (open circles). d, f, h, Relationships between FEV1 (d), WT4 (f), WT5 (h) and the density of $CD45^+$ $FSP1^+$ cells in proximal airways measured in control subjects (black circles) and COPD patients (open circles). The correlation coefficient (r) and significance level (P value) were obtained by using nonparametric Spearman analysis.

Supplementary Fig E8. $CD3^+$ $FSP1^+$ cells represent a minor fraction of $CD45^+$ $FSP1^+$ cells.

a, Representative staining of CD3 (brown, top panels) and FSP1 (green, middle panels) and merged segmented images (CD3, red and FSP1, green, bottom panels) in distal lung tissue from COPD patient. Middle and right columns represent higher magnification of images in

the left column. The yellow arrowheads indicate $CD3^+$ $FSP1^+$ cells. b, d, Quantification of $CD3^+$ $FSP1^+$ cells density (normalized by the sub-epithelial area) in distal (b) and proximal (d) tissue specimens from control subjects and COPD patients. c, e, Comparison of sub-epithelial areas in distal (c) and proximal (e) tissue specimens from control subjects and COPD patients. b-d, The medians are represented as horizontal lines.

Supplementary Fig E9. $CD19^+$ $FSP1^+$ cells are detected neither in proximal and nor in distal airways.

a-b, Representative staining of CD19 (brown, top panels) and FSP1 (green, middle panels) and merged segmented images (CD19, red and FSP1, green, bottom panels) in distal (a) and proximal (b) bronchial tissue specimens from COPD patient. The right columns represent higher magnification of images in the left columns.

Supplementary Fig E10. $CD34^+$ $FSP1^+$ cells are almost absent in distal airways.

a, Representative staining of CD34 (brown, top left panel) and FSP1 (green, bottom left panels) and merged segmented image (CD34, red and FSP1, green, right panel) in distal tissue specimen from COPD patient. The yellow arrowhead indicates $CD34^+$ $FSP1^+$ cells. b, Quantification of $CD34^+$ $FSP1^+$ cells density (normalized by the sub-epithelial area) in distal tissue specimens from control subjects and COPD patients. The medians are represented as horizontal line. c, Percentage of tissue specimens in which $CD34^+$ $FSP1^+$ cells have been detected (density>0, black bars) or undetected (density=0, white bars) in distal tissue specimens from control subjects and COPD patients.

Supplementary Fig E11. $CD34^+$ $FSP1^+$ cells are present at a very low level in proximal airways.

a, Representative staining–of CD34 (brown, top left panel) and FSP1 (green, bottom left panels) and merged segmented image (CD34, red and FSP1, green, right panel) in proximal tissue specimen from COPD patient. The yellow arrowhead indicates $CD34^+$ $FSP1^+$ cells. b, Quantification of $CD34^+$ $FSP1^+$ cells density (normalized by the sub-epithelial area) in proximal tissue specimens from control subjects and COPD patients. The medians are represented as horizontal line. c, Percentage of tissue specimens in which $CD34^+$ $FSP1^+$ cells have been detected (density>0, black bars) or undetected (density=0, white bars) in proximal tissue specimens from control subjects and COPD patients.

Supplementary Fig E12. Relationships between fibrocyte density, lung function parameters and CT parameters within smokers.

a-c, Relationships between FEV1/FVC (a), PaO_2 (b), MLA during expiration (c) and the density of $CD45^+$ $FSP1^+$ cells in distal airways measured in control smokers (black circles) and COPD patients (open circles). d-f, Relationships between FEV1 (d), WT4 (e), WT5 (f) and the density of $CD45^+$ $FSP1^+$ cells in proximal airways measured in control smokers (black circles) and COPD patients (open circles). The correlation coefficient (r) and significance level (P value) were obtained by using nonparametric Spearman analysis.

Supplementary Fig E13. Level of circulating fibrocytes and relationship with tissue fibrocytes density.

a, Level of circulating fibrocytes ($CD45^+$ $ColI^+$ cells), expressed as percentage of PBMC, measured in blood from control subjects ("Cont", n = 22), and COPD patients (“COPD”,

n=12). The medians are represented as horizontal lines. b, Relationships between the level of circulating fibrocytes and the density of $CD45^+$ $FSP1^+$ cells in distal airways measured in control subjects (black circles) and COPD patients (open circles). b, c, The correlation coefficient (r) and significance level (P value) were obtained by using nonparametric Spearman analysis.

Supplementary Fig E14. Influence of epithelium on fibrocyte survival.

a, Representative histograms of flow cytometry for propidium iodide (PI) fluorescence recorded on fibrocytes exposed to epithelium supernatants, either from control subjects (left panel), or COPD patient (right panel). A gate was drawn to define the population of dead cells (PI^+ cells). b, Quantification of PI^+ cells in fibrocytes from COPD patients (n=6) exposed to epithelium supernatants from control subjects (red circles) or COPD patients (blue circles). *: $P<0.05$, Wilcoxon test.

Figure E1

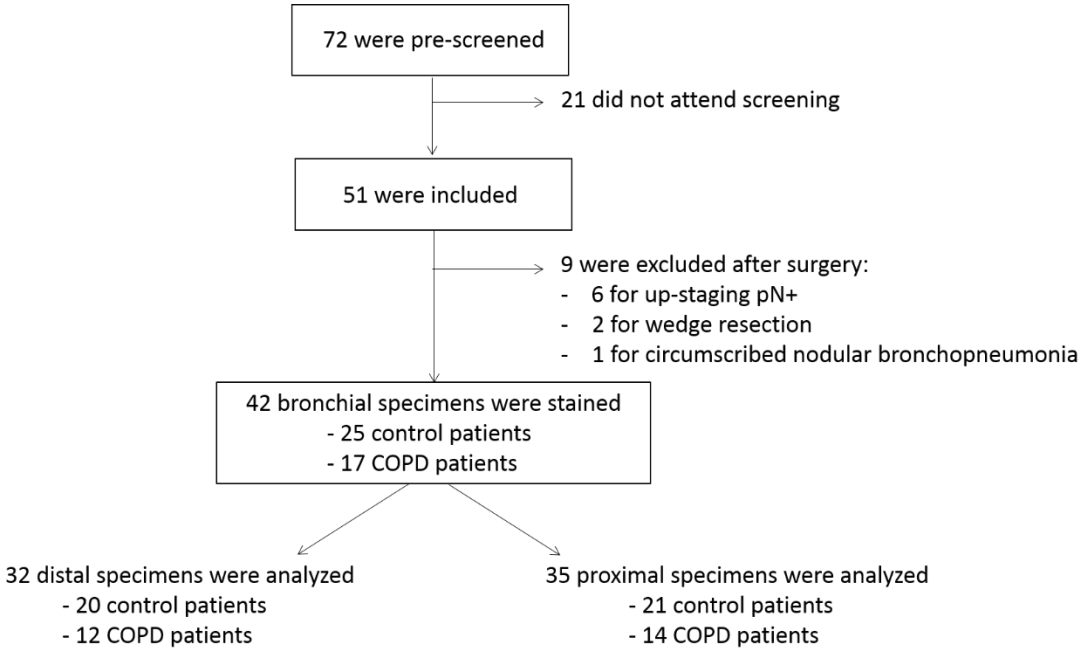
72 were pre-screened
21 did not attend screening
51 were included
9 were excluded after surgery:
- 6 for up-staging pN+
- 2 for wedge resection
- 1 for circumscribed nodular bronchopneumonia
42 bronchial specimens were stained
- 25 control patients
- 17 COPD patients
32 distal specimens were analyzed
- 20 control patients
- 12 COPD patients
35 proximal specimens were analyzed
- 21 control patients
- 14 COPD patients

Figure E2

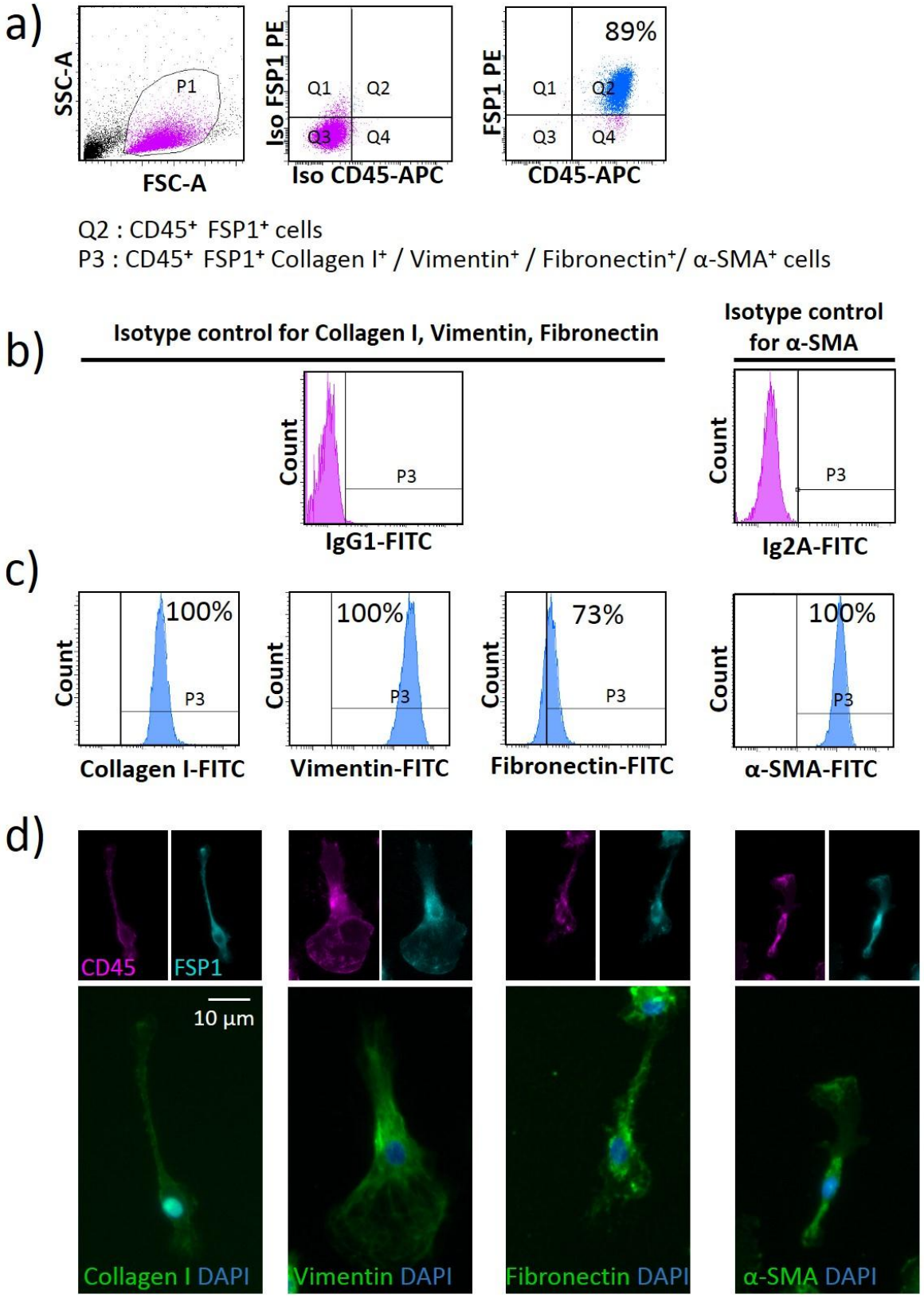
a)
SSC-A
FSC-A
P1
Iso FSP1 PE
Iso CD45-APC
Q1
Q2
Q3
Q4
FSP1 PE
CD45-APC
89%
Q2 : CD45+ FSP1+ cells
P3 : CD45+ FSP1+ Collagen I+ / Vimentin+ / Fibronectin+/ α-SMA+ cells
b)
Isotype control for Collagen I, Vimentin, Fibronectin
Isotype control for α-SMA
Count
P3
IgG1-FITC
Ig2A-FITC
c)
100%
73%
Collagen I-FITC
Vimentin-FITC
Fibronectin-FITC
α-SMA-FITC
d)
CD45
FSP1
10 µm
Collagen I DAPI
Vimentin DAPI
Fibronectin DAPI
α-SMA DAPI

Figure E3

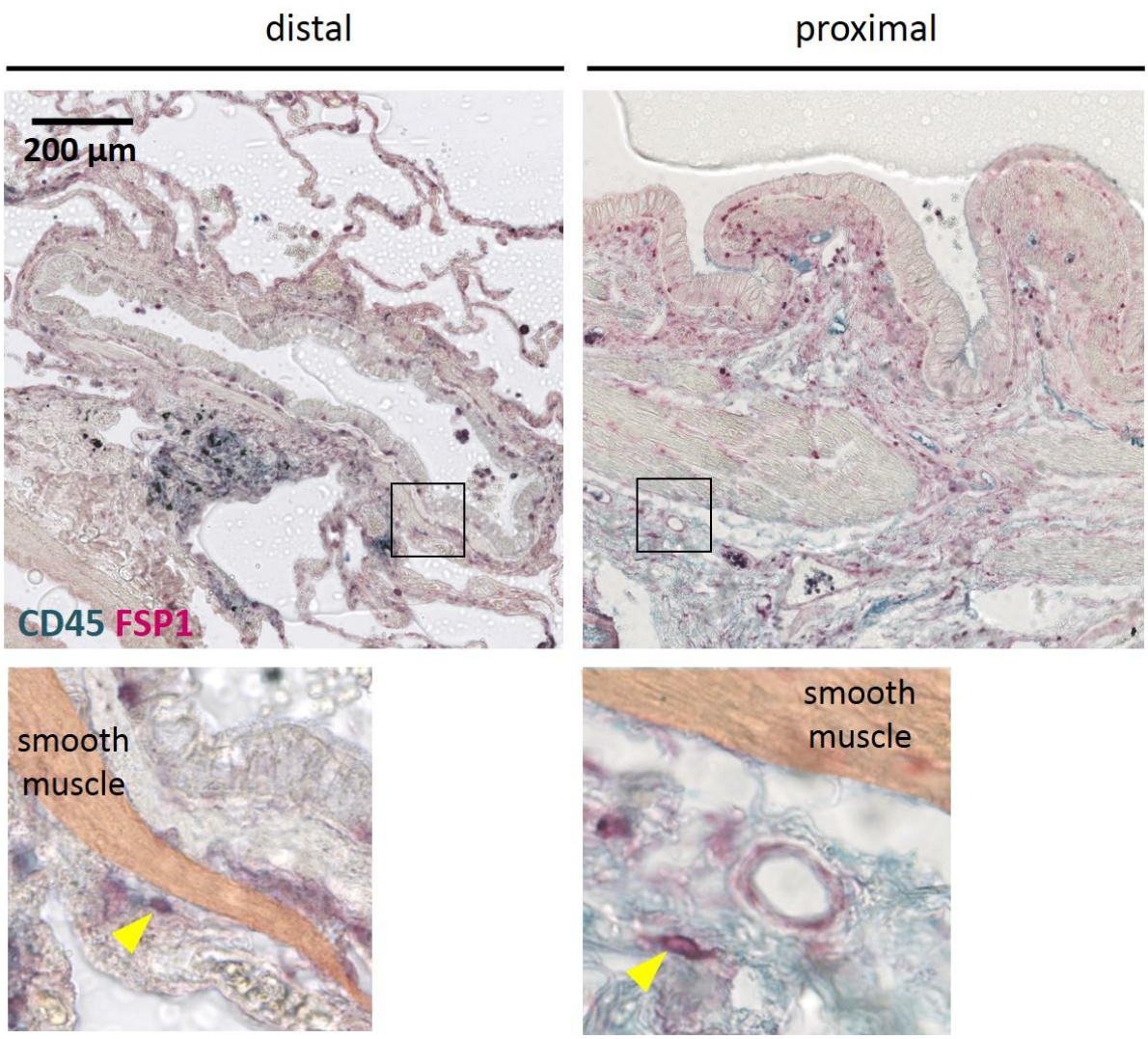
distal
proximal
200 µm
CD45 FSP1
smooth muscle
smooth muscle

Figure E4

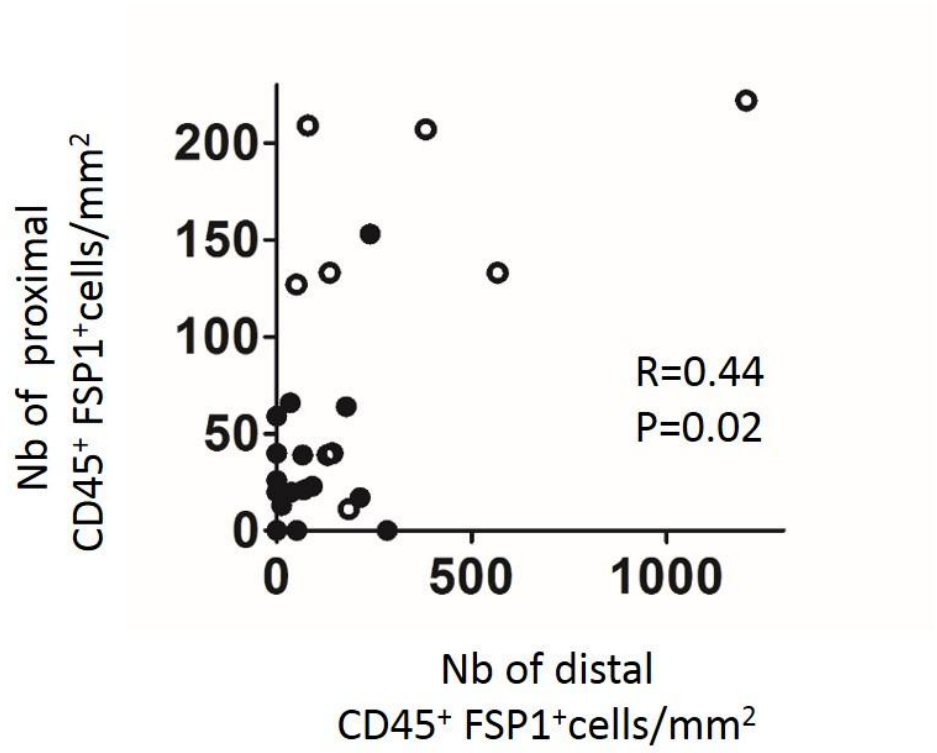
Nb of proximal
CD45+ FSP1+cells/mm2
200
150
100
50
0
0
500
1000
R=0.44
P=0.02
Nb of distal
CD45+ FSP1+cells/mm2

Figure E5

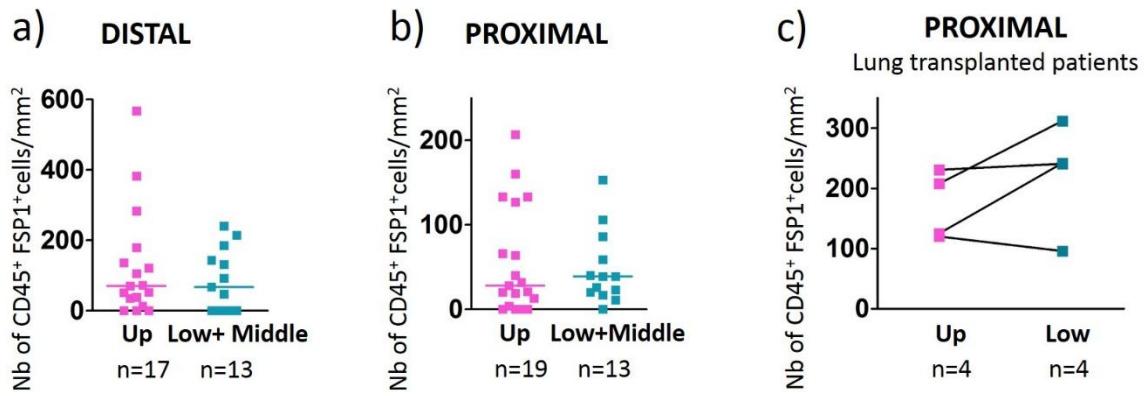
a)
DISTAL
Nb of CD45+ FSP1+cells/mm2
600
400
200
0
Up
Low+ Middle
n=17
n=13
b)
PROXIMAL
Nb of CD45+ FSP1+cells/mm2
200
100
0
Up
Low+Middle
n=19
n=13
c)
PROXIMAL
Lung transplanted patients
Nb of CD45+ FSP1+cells/mm2
300
200
100
0
Up
Low
n=4
n=4

Figure E6

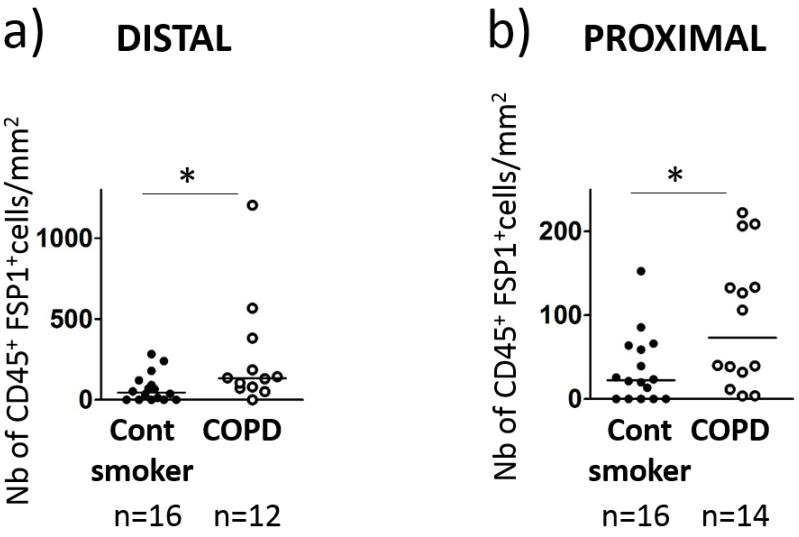
a)
DISTAL
Nb of CD45+ FSP1+cells/mm2
1000
500
0
*
Cont smoker
COPD
n=16
n=12
b)
PROXIMAL
Nb of CD45+ FSP1+cells/mm2
200
100
0
*
Cont smoker
COPD
n=16
n=14

Figure E7

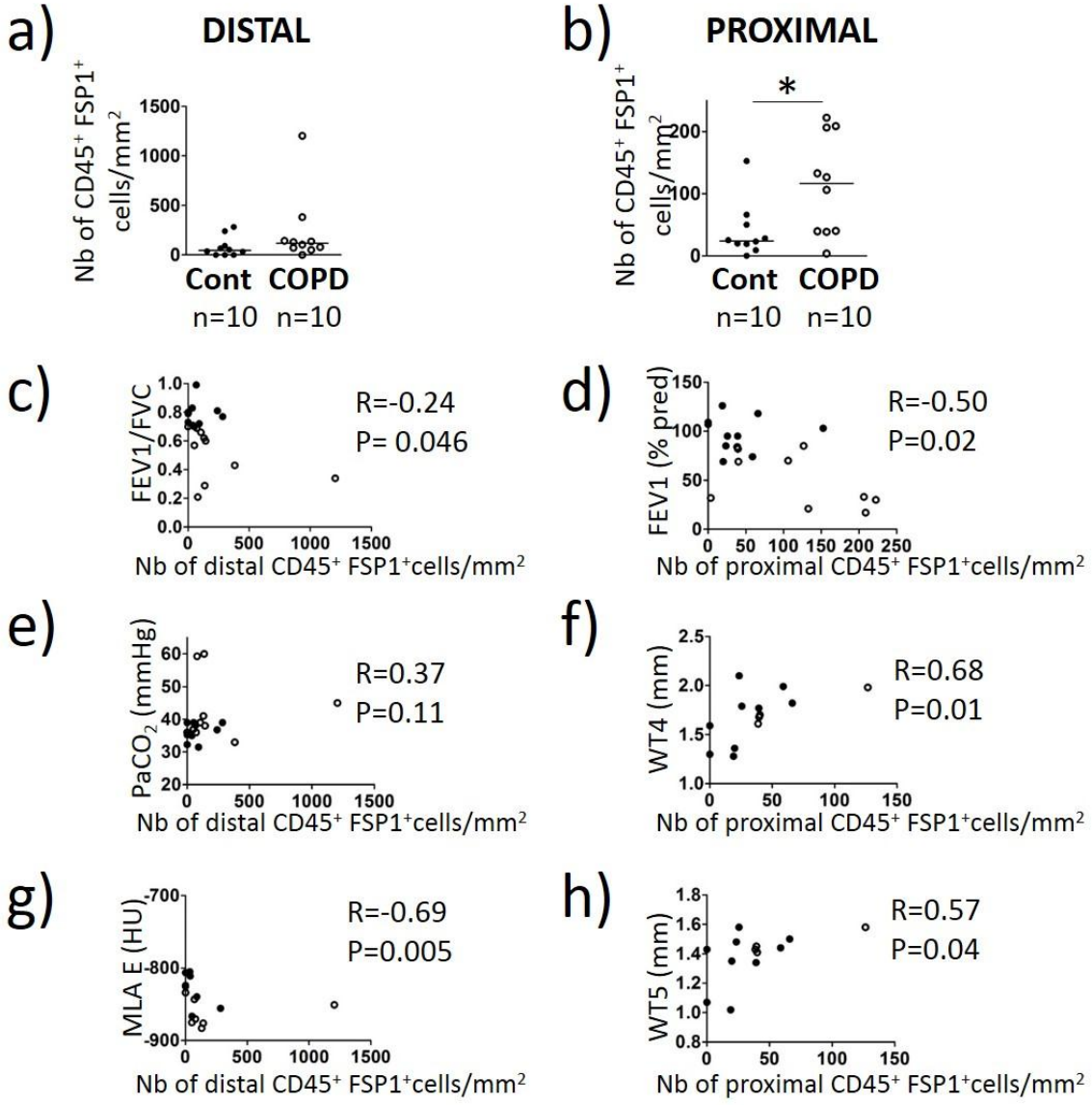
a)
DISTAL
Nb of CD45+ FSP1+ cells/mm2
1500
1000
500
0
Cont
COPD
n=10
n=10
b)
PROXIMAL
Nb of CD45+ FSP1+ cells/mm2
*
200
100
0
Cont
COPD
n=10
n=10
c)
FEV1/FVC
1.0
0.8
0.6
0.4
0.2
0.0
0
500
1000
1500
R=-0.24
P= 0.046
Nb of distal CD45+ FSP1+cells/mm2
d)
FEV1 (% pred)
150
100
50
0
0
50
100
150
200
250
R=-0.50
P=0.02
Nb of proximal CD45+ FSP1+cells/mm2
e)
PaCO2 (mmHg)
60
50
40
30
20
0
500
1000
1500
R=0.37
P=0.11
Nb of distal CD45+ FSP1+cells/mm2
f)
WT4 (mm)
2.5
2.0
1.5
1.0
0
50
100
150
R=0.68
P=0.01
Nb of proximal CD45+ FSP1+cells/mm2
g)
MLA E (HU)
-700
-800
-900
0
500
1000
1500
R=-0.69
P=0.005
Nb of distal CD45+ FSP1+cells/mm2
h)
WT5 (mm)
1.8
1.6
1.4
1.2
1.0
0.8
0
50
100
150
R=0.57
P=0.04
Nb of proximal CD45+ FSP1+cells/mm2

Figure E8

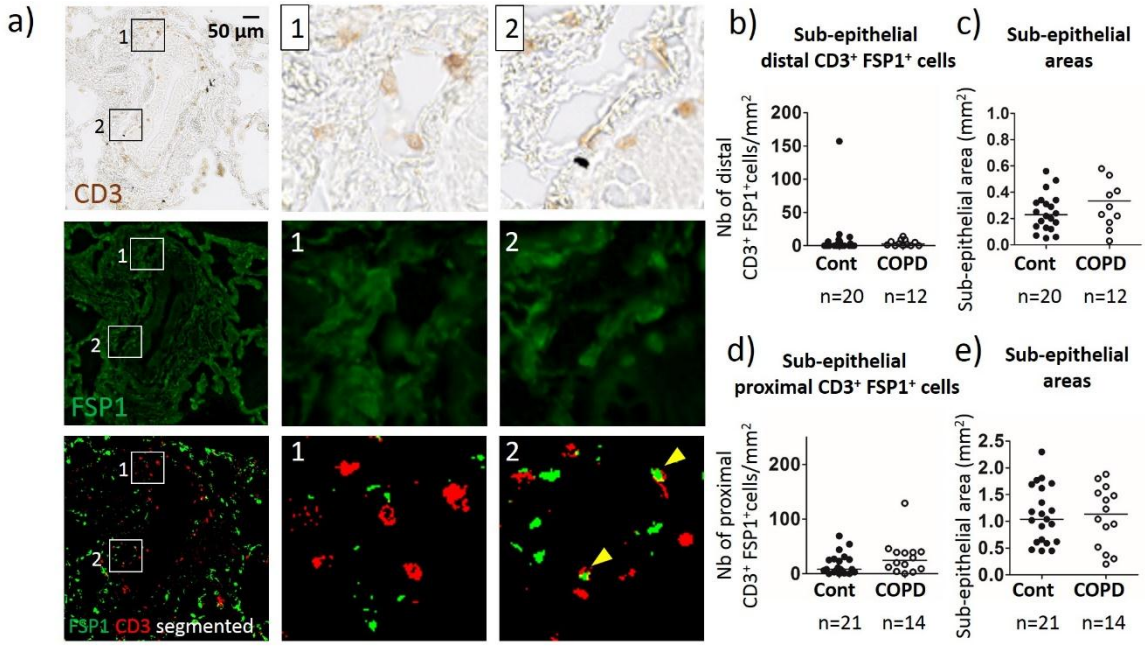
a)
50 µm
CD3
FSP1
FSP1 CD3 segmented
b)
Sub-epithelial distal CD3⁺ FSP1⁺ cells
Nb of distal CD3⁺ FSP1⁺cells/mm²
Cont
COPD
n=20
n=12
c)
Sub-epithelial areas
Sub-epithelial area (mm²)
d)
Sub-epithelial proximal CD3⁺ FSP1⁺ cells
Nb of proximal CD3⁺ FSP1⁺cells/mm²
n=21
n=14
e)
Sub-epithelial areas

Figure E9

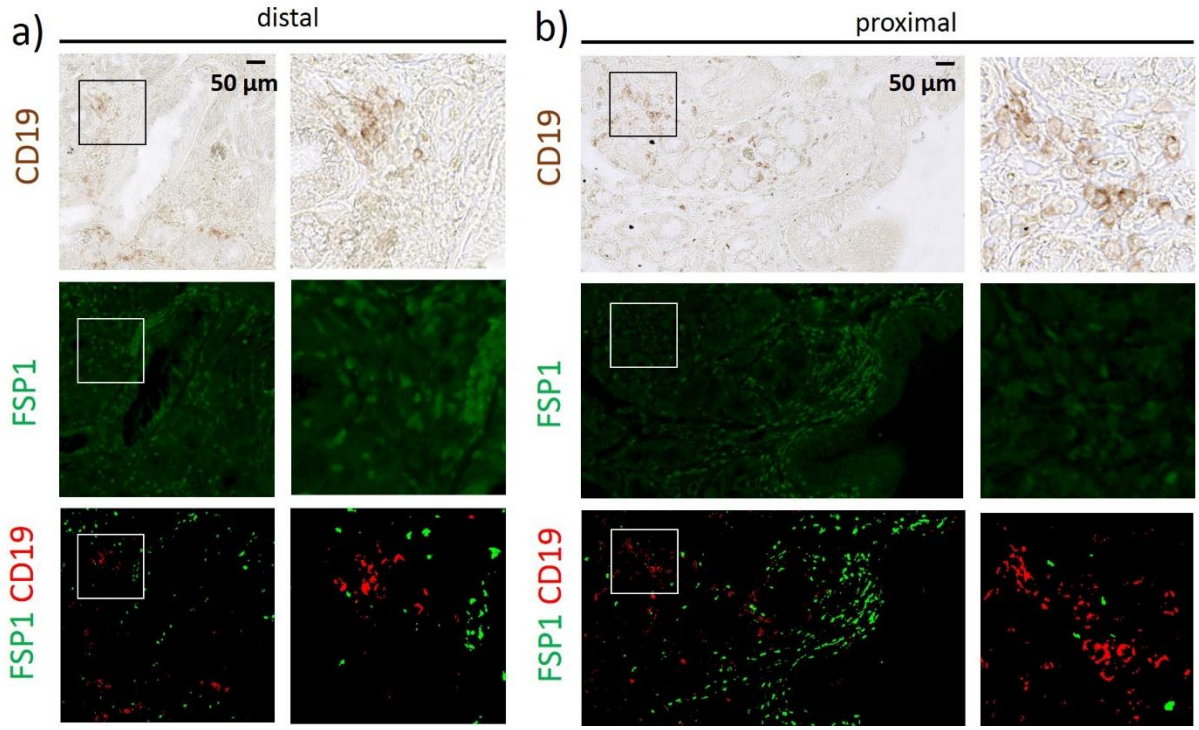

Figure E10

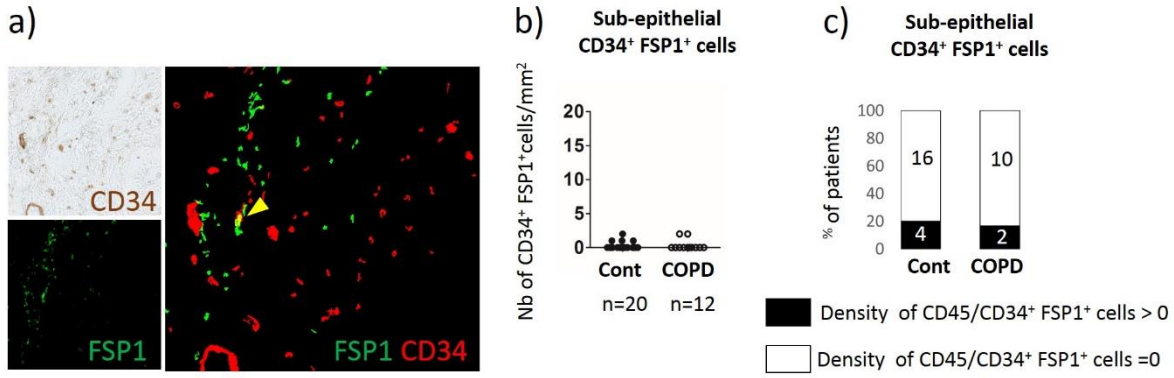
a)
CD34
FSP1
FSP1 CD34
b)
Sub-epithelial
CD34+ FSP1+ cells
Nb of CD34+ FSP1+cells/mm2
20
15
10
5
0
Cont
COPD
n=20
n=12
c)
Sub-epithelial
CD34+ FSP1+ cells
% of patients
100
80
60
40
20
0
16
10
4
2
Cont
COPD
Density of CD45/CD34+ FSP1+ cells > 0
Density of CD45/CD34+ FSP1+ cells =0

Figure E11

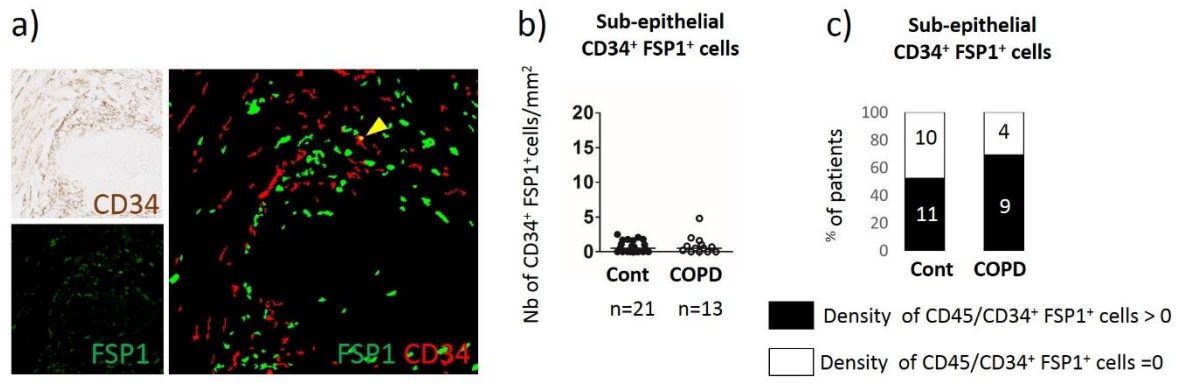
a)
CD34
FSP1
FSP1 CD34
b)
Sub-epithelial
CD34⁺ FSP1⁺ cells
Nb of CD34⁺ FSP1⁺cells/mm²
20
15
10
5
0
Cont
COPD
n=21
n=13
c)
Sub-epithelial
CD34⁺ FSP1⁺ cells
% of patients
100
80
60
40
20
0
10
11
4
9
Cont
COPD
Density of CD45/CD34⁺ FSP1⁺ cells > 0
Density of CD45/CD34⁺ FSP1⁺ cells =0

Figure E12

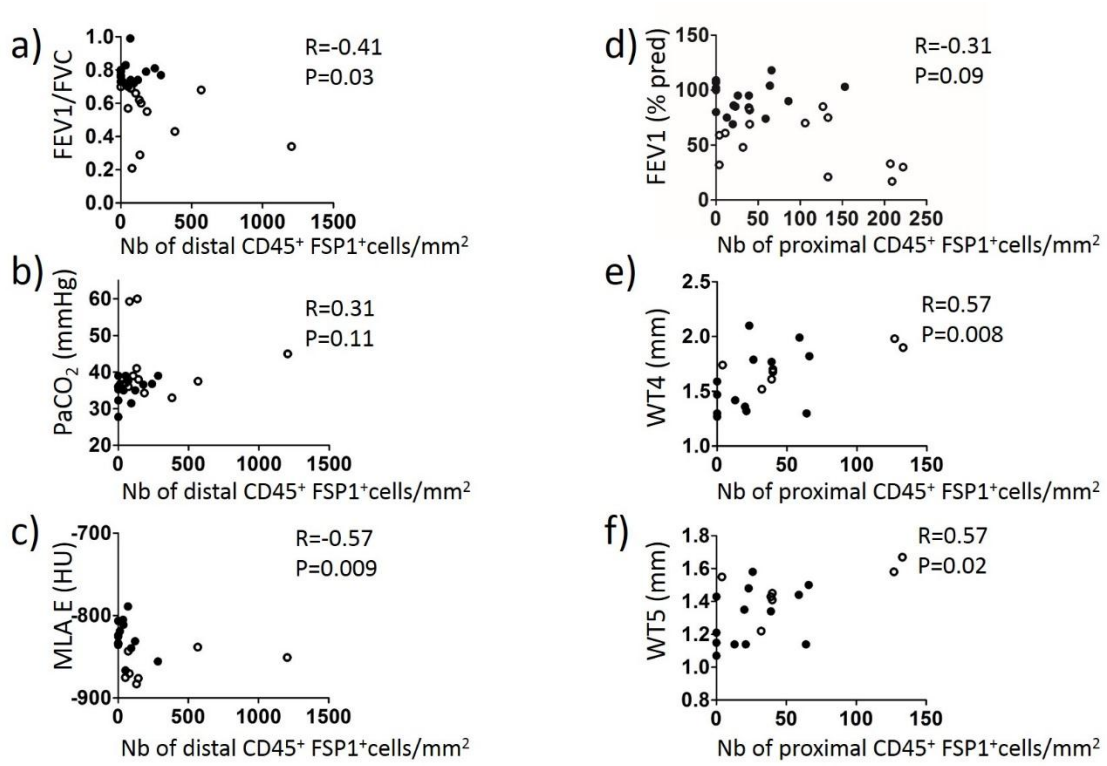
a)
FEV1/FVC
R=-0.41
P=0.03
Nb of distal CD45+ FSP1+cells/mm2
b)
PaCO2 (mmHg)
R=0.31
P=0.11
Nb of distal CD45+ FSP1+cells/mm2
c)
MLA E (HU)
R=-0.57
P=0.009
Nb of distal CD45+ FSP1+cells/mm2
d)
FEV1 (% pred)
R=-0.31
P=0.09
Nb of proximal CD45+ FSP1+cells/mm2
e)
WT4 (mm)
R=0.57
P=0.008
Nb of proximal CD45+ FSP1+cells/mm2
f)
WT5 (mm)
R=0.57
P=0.02
Nb of proximal CD45+ FSP1+cells/mm2

Figure E13

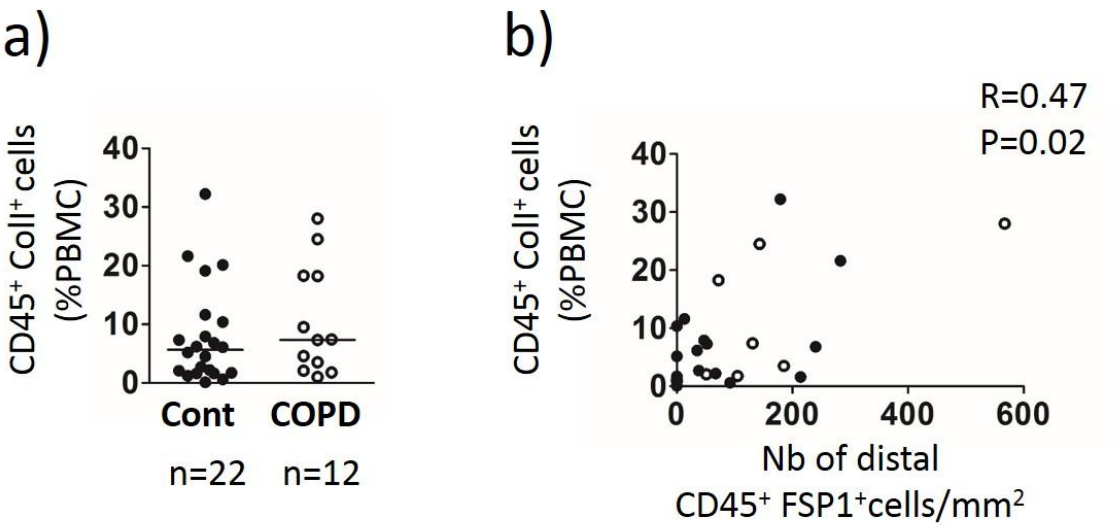
a)
CD45+ CollI+ cells (%PBMC)
40
30
20
10
0
Cont
COPD
n=22
n=12
b)
R=0.47
P=0.02
CD45+ CollI+ cells (%PBMC)
40
30
20
10
0
0
200
400
600
Nb of distal
CD45+ FSP1+cells/mm2

Figure E14

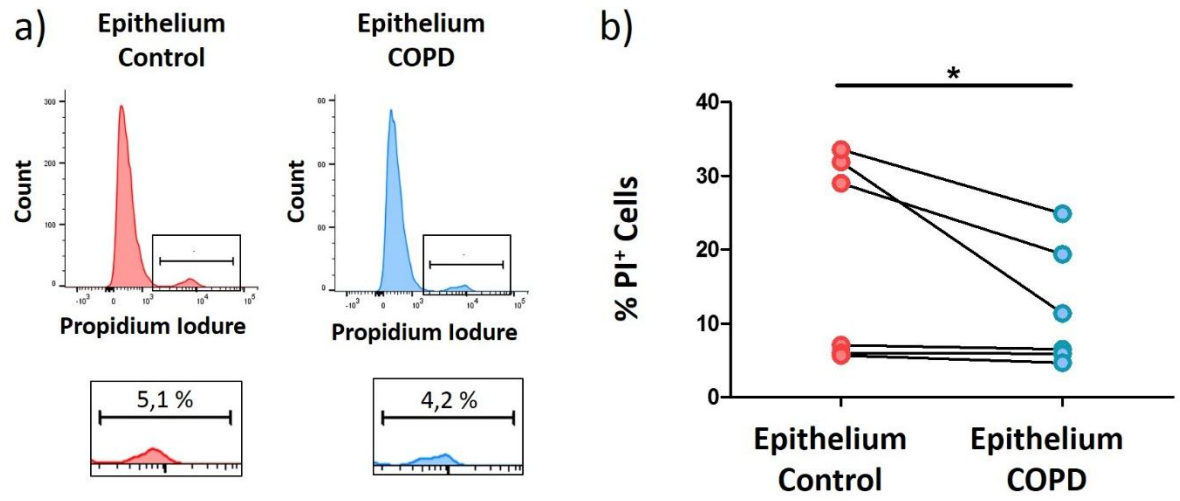
a)
Epithelium Control
Epithelium COPD
Count
Propidium Iodure
5,1 %
4,2 %
b)
*
% PI+ Cells
40
30
20
10
0
Epithelium Control
Epithelium COPD